# Influence of atmospheric in-cloud aqueous-phase chemistry on global simulation of SO₂ in CESM2

Wendong Ge[1], Junfeng Liu[1], Kan Yi[2], Jiayu Xu[1], Yizhou Zhang[1], Xiurong Hu[3], Jianmin Ma[1], Xuejun Wang[1], Yi Wan[1], Jianying Hu[1], Zhaobin Zhang[1], Xilong Wang[1], Shu Tao[1]

5    [1]Laboratory for Earth Surface Processes, College of Urban and Environmental Sciences, Peking University, Beijing, 100871, China

[2]Institute of Science and Technology, China Three Gorges Corporation, Beijing, 100038, China

[3]College of Economics and Management, Nanjing University of Aeronautics and Astronautics, Nanjing, 211106, China

*Correspondence to*: Junfeng Liu (jfliu@pku.edu.cn)

10    **Abstract.** Sulfur dioxide (SO₂) is a major atmospheric pollutant and precursor of sulfate aerosols, which influences air quality, cloud microphysics and climate. Therefore, better understanding the conversion of SO₂ to sulfate is essential to simulate and predict sulfur compounds more accurately. This study evaluates the effects of in-cloud aqueous-phase chemistry on SO₂ oxidation in the Community Earth System Model version 2 (CESM2). We replaced the default aqueous-phase reactions with detailed HO$_x$-, Fe-, N- and carbonate chemistry and performed a global simulation for 2014-2015. Compared with the

15    observations, the results incorporating detailed aqueous-phase chemistry greatly reduced SO₂ overestimation. This overestimation was reduced by 0.1-10 ppbv in most of Europe, North America and Asia and more than 10 ppbv in parts of China. The biases in annual simulated SO₂ concentrations decreased by 46%, 41%, and 22% in Europe, the United States and China, respectively. Fe-chemistry and HO$_x$-chemistry contributed more to SO₂ oxidation than N-chemistry. Higher concentrations of soluble Fe and higher pH values could further enhance the oxidation capacity. This study emphasizes the

20    importance of detailed aqueous-phase chemistry for the oxidation of SO₂. These mechanisms can improve SO₂ simulation in CESM2 and deepen understanding of SO₂ oxidation and sulfate formation.

## 1 Introduction

Sulfur dioxide (SO₂) is one of the major atmospheric pollutants. The anthropogenic emission of SO₂ is the greatest source, which includes mainly the combustion of fossil fuel in the power and steel industries (Buchard et al., 2014). Human health

25    risks from SO₂ have also been discovered and discussed in many studies (Kan et al., 2012;Tong et al., 2017;Chen et al., 2018). More importantly, SO₂ is the precursor of sulfate aerosols. Sulfate can be regarded as one of the core species in the atmosphere. Firstly, it is one of the major components of fine particles (PM₂.₅), which cause haze pollution and affect human health, especially in East and South Asia (Buchard et al., 2014;Chen et al., 2018;Quan et al., 2015;Geng et al., 2019). In addition, sulfate is also the main component of cloud condensation nuclei (CCN), which directly influences the formation of clouds and

30    thus affects precipitation, solar radiation and climate (He et al., 2015a;Tang et al., 2016). Moreover, sulfate itself is also one

of the key species affecting radiative forcing, which directly influences climate change (Li et al., 2018a;Poschl and Shiraiwa, 2015;Xie et al., 2016). Therefore, only through a better understanding of $SO_2$, especially the process of its oxidation to sulfate, can we better understand sulfate and explore all the issues above (Hung et al., 2018).

$SO_2$ can be oxidized to sulfate in multiple ways. On clear and sunny days, the gas-phase oxidation of $SO_2$ by OH radicals ($\cdot OH$)

35    is the dominant pathway (Li et al., 2018a;Cheng et al., 2016). However, when relative humidity (RH) and $PM_{2.5}$ increase on cloudy, foggy or hazy days, solar radiation and photochemical reactions decrease dramatically, resulting in a sharp decrease in gaseous $\cdot OH$ and thus the gas-phase oxidation of $SO_2$, especially in winter. Alternatively, the aqueous-phase oxidation of $SO_2$ becomes much more important because of the increase in atmospheric liquid water content (Cheng et al., 2016;Quan et al., 2015). Aqueous-phase chemistry is an important part of atmospheric chemistry. Various physical and chemical parameters,

40    such as the water content, ionic strength and pH value, could directly affect the gas-aqueous mass transfer process and the reaction rates and then influence the relative contributions of various mechanisms (Elser et al., 2016;Ervens, 2015). For $SO_2$, the aqueous-phase oxidation of $SO_2$ by diverse oxidants can serve as the major sink of atmospheric $SO_2$. It accounts for nearly 80% of global sulfate production, and more than half of sulfate production occurs in clouds (Harris et al., 2013;Huang et al., 2018). Specifically, there are several common oxidation pathways in the aqueous phase, such as oxidation by hydrogen

45    peroxide ($H_2O_2$) and ozone ($O_3$) (Tan et al., 2016;Hung et al., 2018). In recent years, increasing numbers of studies have focused on the catalytic effect of transition metal ions (TMIs) on the aqueous-phase oxidation of $SO_2$ (Tilgner et al., 2013;Alexander et al., 2009). In addition, oxidation by $NO_2$ has also received increasing attention (Xue et al., 2016).

Transition metals in dust particles are important sites for various reactions and affect the moisture absorption, light scattering and nucleation process of clouds. Among these elements, Fe is one of the most important transition metals due to its high

50    abundance and activity (Tang et al., 2016). Soluble Fe can act as an important catalyst in the Fenton reaction for the oxidation of $SO_2$ when dissolved into the aqueous phase. The Fenton reaction, which was firstly proposed by Henry J. H. Fenton in the 1890s, is one of the most important and widespread reactions in multiphase chemistry (Wiegand et al., 2017;Fenton, 1894;Poschl and Shiraiwa, 2015). This reaction involves the production of $\cdot OH$ in the aqueous phase by the decomposition of $H_2O_2$ catalyzed by low-valence TMIs such as $Fe^{2+}$ (Deguillaume et al., 2005;Herrmann et al., 2015). Different mechanisms

55    have been developed to explain the first step of Fenton reactions. Two of the best known pathways are (1) the OH radical mechanism ($Fe^{2+} + H_2O_2 \rightarrow Fe^{3+} + \cdot OH + OH^-$) developed by Haber and Weiss and (2) the non-OH radical mechanism ($Fe^{2+} + H_2O_2 \rightarrow FeO^{2+} + H_2O$) proposed by Bray and Gorin (Fritz and Joseph, 1934;Bray and Gorin, 1932;Wiegand et al., 2017;Poschl and Shiraiwa, 2015). The relative contributions of these two pathways differ under various conditions and remain controversial. A recent experimental study suggested that the non-OH radical mechanism is dominant under nearly neutral

60    conditions (pH $\approx$ 7), while the OH radical mechanism becomes more important under acidic conditions (Pang et al., 2011;Deguillaume et al., 2005;Wiegand et al., 2017;Poschl and Shiraiwa, 2015;Bataineh et al., 2012). Then, all of these oxidative intermediates (i.e., $Fe^{3+}$, $\cdot OH$ and $FeO^{2+}$) can further oxidize $SO_2$ to sulfate. In this way, $Fe^{3+}$ and $FeO^{2+}$ are reduced

to $Fe^{2+}$, thus forming a complete redox cycle. Their concentrations and proportions are basically the same during the redox cycle, and a balance of catalysts is achieved (Deguillaume et al., 2005). The effects of soluble Fe on sulfate formation have

65   been discussed in several studies (Gankanda et al., 2016). In addition, direct oxidation of $SO_2$ by $O_2$ might also be catalyzed by soluble Fe. In general, Fenton reactions could lead to faster radical recycling. The reaction rates of sulfate formation are enhanced with high Fe concentrations, especially when pH < 5 (Shao et al., 2019;Ervens, 2015;Huang et al., 2014;Tilgner et al., 2013).

On the other hand, a number of studies have also emphasized the important role of $NO_2$ in the oxidation of $SO_2$ (Ma et al.,

70   2018;Tao et al., 2017;Huang et al., 2019). He et al. (2014) and Cheng et al. (2016) reported a missing source of $SO_2$ oxidation that can be explained by the synergistic effect between $NO_2$ and $SO_2$ in aerosol water and on mineral dust: $2\ NO_2 + HSO_3^- + H_2O \rightarrow 3\ H^+ + 2\ NO_2^- + SO_4^{2-}$ (He et al., 2014;Cheng et al., 2016). Such a conversion of $SO_2$ by $NO_2$ is driven by a high pH value (e.g., pH > 5.5) and a high concentration of $NO_2$ (Wang et al., 2020;Li et al., 2018b;Huang et al., 2019;He and He, 2020;He et al., 2018). Moreover, these studies have indicated that > 95% of $NO_2$ converts to $HONO/NO_2^-$ to promote the

75   aqueous-phase oxidation of $SO_2$ (Wang et al., 2020;Li et al., 2018b). This pathway can explain the gaps in sulfate concentrations between simulations and observations from approximately 15% to 65% during haze days in winter (Zheng et al., 2020). However, other studies have suggested that the contribution of nitrogen chemistry to $SO_2$ oxidation is very limited. Au Yang et al. (2018) argued that the $NO_2$ oxidation pathway cannot explain the extreme concentrations of sulfate measured in urban aerosols (Au Yang et al., 2018). Only a minor (approximately 2%) fraction of heterogeneous sulfate formation occurs

80   via oxidation of $SO_2$ by $NO_2$ (Shao et al., 2019). The main reason is that the pH value is hardly ever high enough to maintain the efficiency of oxidation by $NO_2$ in aerosol or cloud water (Guo et al., 2017). For instance, aerosols collected from several urban areas in China (CN) were always acidic (even with the unusually high $NH_3$ emissions and concentrations in northern CN), suggesting that oxidation by $NO_2$ might not be very important in these regions (Li et al., 2020;He and He, 2020). In summary, the contribution of N-chemistry to the aqueous-phase oxidation of $SO_2$ still needs further investigation.

85   Many studies have been conducted on the aqueous-phase oxidation of $SO_2$. Some laboratory studies have focused on the detailed mechanism, such as the radical processes involved in different pathways of the Fenton reaction (Wiegand et al., 2017;Bataineh et al., 2012) and the conversion of $NO_2$ to HONO to oxidize $SO_2$ (He et al., 2014). Some studies have paid more attention to the measurement and updating of kinetic parameters (Cwiertny et al., 2008;He et al., 2018;He and He, 2020). More importantly, modelling studies have made great progress in revealing the mechanism of $SO_2$ oxidation and sulfate

90   formation in the aqueous phase (Bell et al., 2005). For instance, Herrmann et al. (2000) used a box model to investigate the detailed aqueous-phase radical mechanism for tropospheric chemistry (Herrmann et al., 2000). Huang et al. (2014) and Li et al. (2017) discussed the enhancement of sulfate formation by mineral aerosols in CN and improved the simulation of heterogeneous sulfate in the WRF-Chem model (Huang et al., 2014;Li et al., 2017). Li et al. (2018a) also improved the simulation of sulfate with the NAQPMS model of oxidation of $SO_2$ by $NO_2$ on wet aerosols on haze days (Li et al., 2018a).

95    Shao et al. (2019) evaluated various heterogeneous mechanisms for sulfate aerosol formation in Beijing using the GEOS-Chem model (Shao et al., 2019). Bell et al. (2005) analyzed the effects of different $SO_2$ emission scenarios on radiative forcing and climate over East Asia (EA) using CESM2 (Bell et al., 2005). Both Zheng et al. (2020) and Zheng et al. (2015) used the CMAQ model to explore heterogeneous chemistry for the formation of secondary inorganic aerosols and the contribution of nitrate photolysis to heterogeneous sulfate formation in CN on winter haze days, respectively (Zheng et al., 2020;Zheng et al., 2015).

100   Zheng et al. (2015) used the WRF-CMAQ model to explain the crucial role of reactive N-chemistry in aerosol water for sulfate formation during haze events in CN (Zheng et al., 2015). Nevertheless, there are still obvious shortcomings in these model studies. First of all, in long-term global climate simulations, studies focused on the spatio-temporal distribution of $SO_2$ concentrations are still insufficient. Most studies have evaluated only sulfate distribution and its climate impact. Very few studies have discussed the simulation of $SO_2$ and these few only from the perspective of $SO_2$ emissions. In addition, although

105   some studies have attempted to discuss different pathways of aqueous-phase oxidation of $SO_2$, most of them have merely adopted simplified mechanisms or even parameterization alone without introducing detailed radical mechanisms. On the other hand, several studies investigated the detailed aqueous-phase chemistry, but they did not analyze its influence on $SO_2$ but discussed that on only $O_3$, ·OH or $HO_2$ (Herrmann et al., 2000;Jacob, 1986;Matthijsen et al., 1995;Jacob, 2000;Mao et al., 2013;Mao et al., 2017). Finally, the simulations of $SO_2$ in many studies are still highly overestimated (He et al., 2015b;He et

110   al., 2015a;Buchard et al., 2014;Hong et al., 2017;Georgiou et al., 2018;Wei et al., 2019;Flemming et al., 2015;Sha et al., 2019;Liu et al., 2012b;Hedegaard et al., 2008), while others underestimate the concentration of sulfate (Xie et al., 2016;Goto et al., 2015;Bell et al., 2005;Lamarque et al., 2012;Pozzer et al., 2012;Guth et al., 2016;Wei et al., 2019;Geng et al., 2019;Kajino et al., 2012;Mathur, 2005;Liu et al., 2012b;Sha et al., 2019;Zhang et al., 2012;Itahashi, 2018). All of these disadvantages indicate that the mechanism of $SO_2$ oxidation to sulfate is still not fully understood.

115   This study, which is divided into five main parts, aims to examine the role played by detailed aqueous-phase chemical mechanisms in the capacity for oxidation of global $SO_2$ with the second version of the Community Earth System Model (CESM2). We describe the CESM2 model, detailed aqueous-phase mechanisms and observational data in Sect. 2. The evaluation of $SO_2$ simulations with or without the coupled detailed aqueous-phase chemistry is given in Sect. 3. The contributions of different aqueous-phase chemical mechanisms to the simulation of $SO_2$ are analyzed in Sect. 4. The factors

120   that affect the capacity for $SO_2$ oxidation are discussed in Sect. 5. Finally, the main conclusions are summarized in Sect. 6.

## 2    Methodology

### 2.1    Model description

The Community Earth System Model 2 (CESM2, v2.1.1), developed by the National Center for Atmospheric Research (NCAR, https://www.cesm.ucar.edu/models/cesm2/, last access: 16 December 2020) is used in this study (Emmons et al.,

125 2020;Danabasoglu et al., 2020), configured with the Community Atmosphere Model version 4.0 (CAM4). The coupled

chemistry in CAM4 is primarily based on the Model for $O_3$ and Related chemical Tracers, version 4 (MOZART-4), including

85 gas-phase species with bulk aerosols and detailed tropospheric chemistry with 196 gas-phase reactions (Emmons et al.,

2010;Lamarque et al., 2012). In this study, we develop a detailed aqueous-phase chemistry module for $SO_2$ coupled in

MOZART-4 chemistry.

130 The model is configured with a horizontal resolution of 0.95° (latitude) × 1.25° (longitude) and 30 levels in the vertical

direction from 993 (near-surface layer) to 3.6 hPa. The model is nudged by assimilated meteorological offline data from

Modern-Era Retrospective analysis for Research and Applications, version 2 (MERRA2, https://rda.ucar.edu/datasets/ds313.3/,

last access: 20 July 2020), prepared with 14 meteorological variables (e.g., air temperature, surface pressure, specific humidity

and eastward and northward winds) to run CESM2 simulations. The meteorological data have a temporal resolution of 3 h.

135 All the emission inventories needed for MOZART-4 chemistry are obtained from the CESM database (https://svn-ccsm-

inputdata.cgd.ucar.edu/trunk/inputdata/atm/cam/chem/, last access: 31 December 2020 ), which was developed for the CMIP6

projects (Feng et al., 2020). The inventories have been updated to 2015, which is the year of the simulation in this study. The

horizontal resolution of these inventories is also 0.95° (latitude) × 1.25° (longitude), matching the resolution of the model.

The variables related to the cloud properties used in this study are all from the Rasch and Kristjansson (RK) prognostic cloud

140 microphysical processes. These variables include the liquid water content of clouds (LWC, $L_{water}$ $L_{air}^{-1}$), volume fraction of

clouds ($F_{cld}$) and radius of cloud droplets (r, μm). They are directly obtained from the model simulation and directly or

indirectly influence the in-cloud aqueous-phase chemistry. Among these variables, the simulated r ranges from 8 μm to 14 μm,

consistent with those in previous studies (Herrmann et al., 2000;Jacob, 1986;Matthijsen et al., 1995;Liu et al., 2012a;Herrmann

et al., 2015). Meanwhile, CESM2 simulates both large-scale stratiform clouds and convective clouds (i.e., shallow cumulus

145 clouds and deep convective clouds). For each type of cloud, both water and ice are simulated. However, the $SO_2$ produced in

convective clouds is assumed to be removed rapidly by convective precipitation. Thus, the contribution of $SO_2$ from shallow

cumulus clouds and deep convective clouds is ignored. Only the LWC and $F_{cld}$ of large-scale liquid stratiform clouds are

employed in this study.

## 2.2 Mechanism of in-cloud aqueous-phase oxidation of $SO_2$

150 The detailed mechanism of in-cloud aqueous-phase oxidation of $SO_2$ is divided into the gas-aqueous phase transfer process

and aqueous-phase chemical mechanisms, listed in Tables 1a and 1b, respectively (see below). There are 32 (16 pairs of) gas-

aqueous phase transfer equilibria and 187 aqueous-phase reactions (only in cloud droplets, not on aerosol surfaces), involving

46 new aqueous species in all. Specifically, the aqueous-phase reactions include 26 (13 pairs of) ionization equilibria and four

different chemistry modules, which are $HO_x$-chemistry, Fe-chemistry, N-chemistry and carbonate chemistry. The aqueous-

155 phase oxidation of $SO_2$ by $H_2O_2$ and $O_3$ is included in the $HO_x$-chemistry mechanism. The two pathways of the Fenton reaction

are included in the Fe-chemistry mechanism. The aqueous-phase oxidation of $SO_2$ by $NO_2$ is included in the N-chemistry mechanism.

**Table 1a:  Gas-aqueous phase transfer equilibria.**

| No. | Reactions | $k_1$ | Reference | $k_2$ | Reference |
|---|---|---|---|---|---|
| | Gas-aqueous phase transfer | | | | |
| 1[a,c] | $O_3(g) \rightarrow O_3$ | 48 | | 0.05 | a |
| 2[b] | $O_3 \rightarrow O_3(g)$ | $1.1 \times 10^{-2}$ | b | -5.075 | c |
| 3[a] | $HO_2(g) \rightarrow HO_2$ | 33 | | 0.01 | a |
| 4[b] | $HO_2 \rightarrow HO_2(g)$ | $9.0 \times 10^3$ | a | 0 | a |
| 5[a] | $OH(g) \rightarrow OH$ | 17 | | 0.05 | a |
| 6[b] | $OH \rightarrow OH(g)$ | 25 | a | -10.5 | b |
| 7[a] | $H_2O_2(g) \rightarrow H_2O_2$ | 34 | | 0.11 | a |
| 8[b] | $H_2O_2 \rightarrow H_2O_2(g)$ | $1.02 \times 10^5$ | a | -12.68 | a |
| 9[a] | $SO_2(g) \rightarrow SO_2$ | 64 | | 0.13 | d |
| 10[b] | $SO_2 \rightarrow SO_2(g)$ | 1.2 | b | -6.27 | b |
| 11[a] | $CO_2(g) \rightarrow CO_2$ | 44 | | $2 \times 10^{-4}$ | a |
| 12[b] | $CO_2 \rightarrow CO_2(g)$ | $3.11 \times 10^{-2}$ | a | -4.84 | a |
| 13[a] | $NH_3(g) \rightarrow NH_3$ | 17 | | 0.04 | a |
| 14[b] | $NH_3 \rightarrow NH_3(g)$ | 60.7 | a | -7.84 | a |
| 15[a] | $HNO_3(g) \rightarrow HNO_3$ | 63 | | 0.054 | a |
| 16[b] | $HNO_3 \rightarrow HNO_3(g)$ | $2.1 \times 10^5$ | a | -17.39 | a |
| 17[a] | $HCOOH(g) \rightarrow HCOOH$ | 46 | | 0.012 | a |
| 18[b] | $HCOOH \rightarrow HCOOH(g)$ | $5.53 \times 10^3$ | a | -11.26 | a |
| 19[a] | $CH_3COOH(g) \rightarrow CH_3COOH$ | 60 | | 0.019 | a |
| 20[b] | $CH_3COOH \rightarrow CH_3COOH(g)$ | $5.50 \times 10^3$ | a | -11.79 | a |
| 21[a] | $NO_3(g) \rightarrow NO_3$ | 62 | | $4 \times 10^{-3}$ | a |
| 22[b] | $NO_3 \rightarrow NO_3(g)$ | 0.6 | a | 0 | a |
| 23[a] | $N_2O_5(g) \rightarrow N_2O_5$ | 108 | | $3.7 \times 10^{-3}$ | a |
| 24[b] | $N_2O_5 \rightarrow N_2O_5(g)$ | 1.4 | a | 0 | a |
| 25[a] | $NO_2(g) \rightarrow NO_2$ | 46 | | $1.5 \times 10^{-3}$ | a |
| 26[b] | $NO_2 \rightarrow NO_2(g)$ | $1.0 \times 10^{-2}$ | c | -5.03 | c |
| 27[a] | $HO_2NO_2(g) \rightarrow HO_2NO_2$ | 79 | | 0.1 | a |
| 28[b] | $HO_2NO_2 \rightarrow HO_2NO_2(g)$ | $1 \times 10^5$ | a | 0 | a |
| 29[a] | $NO(g) \rightarrow NO$ | 30 | | 0.1 | Estimated |
| 30[b] | $NO \rightarrow NO(g)$ | $1.9 \times 10^{-3}$ | c | -2.92 | c |
| 31[a] | $O_2(g) \rightarrow O_2$ | 32 | | 0.1 | Estimated |
| 32[b] | $O_2 \rightarrow O_2(g)$ | $1.3 \times 10^{-3}$ | c | 0 | c |

160    [a] Reaction rate constant $k = \frac{3 \, D_g \, LWC}{\Lambda \, r^2}$. The unit is s$^{-1}$. Gas phase diffusion coefficient $D_g = \frac{9.45 \times 10^{17}}{[M]} \sqrt{T \left( 0.03472 + \frac{1}{k_1} \right)}$. LWC is the volume

mixing ratio of cloud liquid water. $\Lambda = 1 + \left( \lambda + 1.3 \left( \frac{1}{k_2} - 1 \right) \right)$, $\lambda = \frac{0.71 + 1.3\beta}{1 + \beta}$, $\beta = 4.54 \times 10^{-15} \sqrt{V_g^2 + V_{air}^2}$, $V_g = \sqrt{\frac{8RT}{\pi k_1}}$, $V_{air} =$

$\sqrt{\frac{8RT}{28.8\pi}}$, $R = 8.31 \times 10^7$ is the ideal gas constant (multiplied by a factor to keep $V_g$ and $V_{air}$ in the unit of cm s$^{-1}$), r is the radius of cloud

droplets in cm, [M] is the number density of air in the unit of molecules cm$^{-3}$. T is temperature in Kelvin. All the formulas above refer to

(Shao et al., 2019;Liang and Jacobson, 1999).

165   [b] Reaction rate constant $k = \frac{k_{n-1}}{0.082 \, T \, LWC \, C}$. The unit is s⁻¹. $C = k_1 exp\left(-500k_2\left(\frac{1}{T} - \frac{1}{298}\right)\right)$, $k_{n-1}$ is the rate constant of its reverse reaction

with [a]. LWC is as in [a]. All the formulas above refer to (Liang and Jacobson, 1999).

[c] All species are liquid species by default, and gas species are marked with (g).

**Table 1b.  Aqueous-phase chemistry.**

| No. | Reactions | $k_{298}$, M⁻ⁿ s⁻¹ [a] | $E_a/R$, K | Reference |
|---|---|---|---|---|
| | Aqueous ionization equilibria | | | |
| 33 | $H_2O_2 \rightarrow H^+ + HO_2^-$ | $1.26 \times 10^{-2}$ | | e |
| 34 | $H^+ + HO_2^- \rightarrow H_2O_2$ | $10^{10}$ | | e |
| 35 | $HO_2 \rightarrow H^+ + O_2^-$ | $1.14 \times 10^6$ | | e |
| 36 | $H^+ + O_2^- \rightarrow HO_2$ | $7.2 \times 10^{10}$ | | e |
| 37 | $CO_2 + H_2O \rightarrow H^+ + HCO_3^-$ | $3.84 \times 10^4$ | 9250 | a |
| 38 | $H^+ + HCO_3^- \rightarrow CO_2 + H_2O$ | $5 \times 10^{10}$ | | a |
| 39 | $HCO_3^- \rightarrow H^+ + CO_3^{2-}$ | 2.35 | 1820 | a |
| 40 | $H^+ + CO_3^{2-} \rightarrow HCO_3^-$ | $5 \times 10^{10}$ | | a |
| 41 | $NH_3 + H_2O \rightarrow NH_4^+ + OH^-$ | $6.02 \times 10^5$ | 560 | a |
| 42 | $NH_4^+ + OH^- \rightarrow NH_3 + H_2O$ | $3.4 \times 10^{10}$ | | a |
| 43 | $HNO_3 \rightarrow H^+ + NO_3^-$ | $1.1 \times 10^{12}$ | -1800 | a |
| 44 | $H^+ + NO_3^- \rightarrow HNO_3$ | $5 \times 10^{10}$ | | a |
| 45 | $HNO_2 \rightarrow H^+ + NO_2^-$ | $2.65 \times 10^7$ | 1760 | a |
| 46 | $H^+ + NO_2^- \rightarrow HNO_2$ | $5 \times 10^{10}$ | | a |
| 47 | $HO_2NO_2 \rightarrow H^+ + O_2NO_2^-$ | $5 \times 10^5$ | | a |
| 48 | $H^+ + O_2NO_2^- \rightarrow HO_2NO_2$ | $5 \times 10^{10}$ | | a |
| 49 | $SO_2 + H_2O \rightarrow H^+ + HSO_3^-$ | $6.27 \times 10^4$ | -1940 | a |
| 50 | $H^+ + HSO_3^- \rightarrow SO_2 + H_2O$ | $2.0 \times 10^8$ | | a |
| 51 | $HSO_3^- \rightarrow H^+ + SO_3^{2-}$ | 3110 | -1960 | a |
| 52 | $H^+ + SO_3^{2-} \rightarrow HSO_3^-$ | $5 \times 10^{10}$ | | a |
| 53 | $HSO_4^- \rightarrow H^+ + SO_4^{2-}$ | $1.02 \times 10^9$ | -2700 | a |
| 54 | $H^+ + SO_4^{2-} \rightarrow HSO_4^-$ | $1 \times 10^{11}$ | | a |
| 55 | $HCOOH \rightarrow H^+ + HCOO^-$ | $8.85 \times 10^6$ | -12 | a |
| 56 | $H^+ + HCOO^- \rightarrow HCOOH$ | $5 \times 10^{10}$ | | a |
| 57 | $CH_3COOH \rightarrow H^+ + CH3COO^-$ | $8.75 \times 10^5$ | -46 | a |
| 58 | $H^+ + CH3COO^- \rightarrow CH_3COOH$ | $5 \times 10^{10}$ | | a |
| | | | | |
| | HO$_x$-chemistry | | | |
| 59 | $H_2O_2 \xrightarrow{hv} 2\,OH$ | See ref. | | f |
| 60 | $O_3 \xrightarrow{H_2O,hv} H_2O_2 + O_2$ | See ref. | | g |
| 61 | $OH + HO_2 \rightarrow H_2O + O_2$ | $6.6 \times 10^9$ | 1500 | b |
| 62 | $HO_2 + HO_2 \rightarrow H_2O_2 + O_2$ | $8.3 \times 10^5$ | 2700 | b |
| 63 | $OH + H_2O_2 \rightarrow HO_2 + H_2O$ | $2.7 \times 10^7$ | 1700 | b |
| 64 | $O_2^- + O_3 \xrightarrow{H_2O} OH + OH^- + 2\,O_2$ | $1.5 \times 10^9$ | 1500 | b |
| 65 | $OH + HSO_3^- \xrightarrow{O_2} SO_5^- + H_2O$ | $4.5 \times 10^9$ | 1500 | b |
| 66 | $OH + SO_3^{2-} \xrightarrow{O_2} SO_5^- + OH^-$ | $5.5 \times 10^9$ | 1500 | b |
| 67 | $HCOO^- + OH \xrightarrow{O_2} CO_2 + HO_2 + OH^-$ | $3.2 \times 10^9$ | 1250 | b |

| 68 | $SO_3^{2-} + SO_4^- \xrightarrow{O_2} SO_4^{2-} + SO_5^-$ | $7.5 \times 10^8$ | 1500 | b |
|---|---|---|---|---|
| 69 | $HSO_3^- + SO_4^- \xrightarrow{O_2} SO_4^{2-} + SO_5^- + H^+$ | $7.5 \times 10^8$ | 1500 | b |
| 70 | $HSO_3^- + O_3 \rightarrow SO_4^{2-} + H^+ + O_2$ | $3.7 \times 10^5$ | 5530 | b |
| 71 | $SO_3^{2-} + O_3 \rightarrow SO_4^{2-} + O_2$ | $1.5 \times 10^9$ | 5280 | b |
| 72 | $SO_4^- + OH^- \rightarrow SO_4^{2-} + OH$ | $8.0 \times 10^7$ | 1500 | b |
| 73 | $SO_4^- + H_2O_2 \rightarrow H^+ + SO_4^{2-} + HO_2$ | $1.2 \times 10^7$ | 2000 | b |
| 74 | $SO_4^- (+ H_2O) \rightarrow SO_4^{2-} + H^+ + OH$ | 440 | 1850 | b |
| 75 | $SO_4^- + HCOO^- \xrightarrow{O_2} SO_4^{2-} + CO_2 + HO_2$ | $1.1 \times 10^8$ | 1500 | b |
| 76 | $HCOOH + OH \xrightarrow{O_2} H_2O + CO_2 + HO_2$ | $1.1 \times 10^8$ | 1000 | b |
| 77 | $O_3 + H_2O_2 + OH^- \rightarrow OH + O_2^- + O_2 + H_2O$ | $4.4 \times 10^8$ | -4000 | b |
| 78 | $SO_4^- + HO_2 \rightarrow SO_4^{2-} + H^+ + O_2$ | $5.0 \times 10^9$ | 1500 | b |
| 79 | $SO_4^- + O_2^- \rightarrow SO_4^{2-} + O_2$ | $5.0 \times 10^9$ | 1500 | b |
| 80 | $HCOO^- + O_3 \rightarrow CO_2 + OH + O_2^-$ | $1.0 \times 10^2$ | 5500 | b |
| 81 | $SO_5^- + HCOO^- \xrightarrow{O_2} HSO_5^- + CO_2 + O_2^-$ | $1.4 \times 10^4$ | 4000 | b |
| 82 | $SO_5^- + HSO_3^- \xrightarrow{O_2} HSO_5^- + SO_5^-$ | $2.5 \times 10^4$ | 3850 | b |
| 83 | $HSO_5^- + OH \rightarrow SO_5^- + H_2O$ | $1.7 \times 10^7$ | 1900 | b |
| 84 | $HSO_5^- + HSO_3^- + H^+ \rightarrow 2\,SO_4^{2-} + 3\,H^+$ | $1.7 \times 10^7$ | 2000 | b |
| 85 | $SO_5^- + HSO_3^- \rightarrow SO_4^- + SO_4^{2-} + H^+$ | $7.5 \times 10^4$ | 3500 | b |
| 86 | $O_2^- + SO_5^- \xrightarrow{H_2O} O_2 + HSO_5^- + OH^-$ | $1.0 \times 10^8$ | 1050 | b |
| 87 | $OH + HSO_3^- \xrightarrow{O_2} SO_4^{2-} + H^+$ | $4.5 \times 10^9$ | | h |
| 88 | $OH + O_3 \rightarrow HO_2 + O_2$ | $2.0 \times 10^9$ | | h |
| 89 | $HO_2 + O_2^- \xrightarrow{H^+} H_2O_2 + O_2$ | $9.7 \times 10^7$ | 1060 | a |
| 90 | $O_2^- + OH \rightarrow OH^- + O_2$ | $1.1 \times 10^{10}$ | 2120 | a |
| 91 | $HSO_3^- + OH \rightarrow H_2O + SO_3^-$ | $2.7 \times 10^9$ | | a |
| 92 | $SO_3^{2-} + OH \rightarrow OH^- + SO_3^-$ | $4.6 \times 10^9$ | | a |
| 93 | $HSO_3^- + H_2O_2 + H^+ \rightarrow SO_4^{2-} + H_2O + 2\,H^+$ | $6.9 \times 10^7$ | 4000 | a |
| 94 | $SO_2 + O_3 \xrightarrow{H_2O} HSO_4^- + O_2 + H^+$ | $2.4 \times 10^4$ | | a |
| 95 | $SO_5^- + SO_5^- \rightarrow S_2O_8^{2-} + O_2$ | $1.8 \times 10^8$ | 2600 | a |
| 96 | $SO_5^- + SO_5^- \rightarrow 2\,SO_4^- + O_2$ | $7.2 \times 10^6$ | 2600 | a |
| 97 | $SO_5^- + HO_2 \rightarrow HSO_5^- + O_2$ | $1.7 \times 10^9$ | | a |
| 98 | $SO_3^- + O_2 \rightarrow SO_5^-$ | $2.5 \times 10^9$ | | a |
| 99 | $SO_5^- + HSO_3^- \rightarrow HSO_5^- + SO_3^-$ | $8.6 \times 10^3$ | | a |
| 100 | $SO_5^- + SO_3^{2-} \xrightarrow{H^+} HSO_5^- + SO_3^-$ | $2.13 \times 10^5$ | | a |
| 101 | $SO_5^- + SO_3^{2-} \rightarrow SO_4^- + SO_4^{2-}$ | $5.5 \times 10^5$ | | a |
| 102 | $OH + HSO_4^- \rightarrow H_2O + SO_4^-$ | $3.5 \times 10^5$ | | a |
| 103 | $SO_4^- + HSO_3^- \rightarrow SO_4^{2-} + SO_3^- + H^+$ | $3.2 \times 10^8$ | | a |
| 104 | $SO_4^- + SO_3^{2-} \rightarrow SO_4^{2-} + SO_3^-$ | $3.2 \times 10^8$ | 1200 | a |
| 105 | $HSO_5^- + SO_3^{2-} + H^+ \rightarrow 2\,SO_4^{2-} + 2\,H^+$ | $7.14 \times 10^6$ | | a |
| 106 | $HCOOH + SO_4^- \xrightarrow{O_2} SO_4^{2-} + H^+ + HO_2 + CO_2$ | $2.5 \times 10^6$ | | a |
| 107 | $O_2^- + H_2O_2 \rightarrow OH^- + OH + O_2$ | 0.13 | | e |
| 108 | $OH + OH \rightarrow H_2O_2$ | $5.5 \times 10^9$ | | e |
| 109 | $H_2O_2 + HO_2 \rightarrow H_2O + O_2 + OH$ | 3.1 | | e |
| 110 | $HO_2 + O_2^- \rightarrow HO_2^- + O_2$ | $9.7 \times 10^7$ | | e |
| 111 | $O_2^{2-} + H^+ \rightarrow HO_2^-$ | $10^{10}$ | | e |
| 112 | $SO_4^- + SO_4^- \rightarrow S_2O_8^{2-}$ | $4.5 \times 10^8$ | | c |
| 113 | $OH^- + O_3 \xrightarrow{H_2O} H_2O_2 + O_2 + OH^-$ | 70 | | c |
| 114 | $HO_2^- + O_3 \rightarrow OH + O_2^- + O_2$ | $2.8 \times 10^6$ | 2500 | c |

| | | | | |
|---|---|---|---|---|
| 115 | $H_2O_2 + O_3 \rightarrow H_2O + 2\,O_2$ | $7.8 \times 10^{-3}\,[O_3]^{-0.5}$ | | c |
| 116 | $HCOOH + O_3 \rightarrow CO_2 + HO_2 + OH$ | 5.0 | 0 | c |
| 117 | $SO_2 + H_2O_2 \xrightarrow{H_2O} SO_4^{2-} + 2\,H^+ + H_2O$ | $7.5 \times 10^7$ | 4430 | c |
| 118 | $SO_3^{2-} + H_2O_2 \rightarrow SO_4^{2-} + H_2O$ | $7.5 \times 10^7$ | 4430 | c |
| 119 | $SO_5^- + SO_3^{2-} \xrightarrow{O_2,H_2O} HSO_5^- + SO_5^- + OH^-$ | $2.5 \times 10^4$ | 2000 | c |
| 120 | $SO_5^- + HCOOH \xrightarrow{O_2} HSO_5^- + CO_2 + HO_2$ | 200 | 5300 | c |
| 121 | $SO_2 + HO_2 \xrightarrow{H_2O} SO_4^{2-} + OH + 2\,H^+$ | $1.0 \times 10^6$ | 0 | c |
| 122 | $HSO_3^- + HO_2 \rightarrow SO_4^{2-} + OH + H^+$ | $1.0 \times 10^6$ | 0 | c |
| 123 | $SO_3^{2-} + HO_2 \rightarrow SO_4^{2-} + OH$ | $1.0 \times 10^6$ | 0 | c |
| 124 | $SO_2 + O_2^- \xrightarrow{H_2O} SO_4^{2-} + OH + H^+$ | $1.0 \times 10^5$ | 0 | c |
| 125 | $HSO_3^- + O_2^- \rightarrow SO_4^{2-} + OH$ | $1.0 \times 10^5$ | 0 | c |
| 126 | $SO_3^{2-} + O_2^- \xrightarrow{H_2O} SO_4^{2-} + OH + OH^-$ | $1.0 \times 10^5$ | 0 | c |
| 127 | $SO_3^- + SO_3^- \xrightarrow{H_2O} SO_3^{2-} + H^+ + HSO_4^-$ | 0.37 | | i |
| | **Fe-chemistry** | | | |
| 128 | $FeOH^{2+} \xrightarrow{h\nu} Fe^{2+} + OH$ | See ref. | | g |
| 129 | $FeSO_4^+ \xrightarrow{h\nu} Fe^{2+} + SO_4^-$ | See ref. | | a |
| 130 | $H_2O_2 + Fe^{2+} \rightarrow FeOH^{2+} + OH$ | $63 + (3 \times 10^{-10}\,[H^+]^{-1}\,5.9 \times 10^6)$ | | h |
| 131 | $Fe^{2+} + O_3 \xrightarrow{H_2O} FeOH^{2+} + OH + O_2$ | $8.2 \times 10^5$ | | h |
| 132 | $FeOH^{2+} + HSO_3^- \xrightarrow{O_2} Fe^{2+} + SO_4^{2-} + H_2O$ | $[FeOH^{2+}] \times 1 \times 10^9$ | | h |
| 133 | $O_3 + Fe^{2+} \rightarrow FeO^{2+} + O_2$ | $8.2 \times 10^5$ | | j |
| 134 | $H_2O_2 + FeO^{2+} \rightarrow FeOH^{2+} + HO_2$ | $9.2 \times 10^3$ | 2800 | j |
| 135 | $HO_2 + FeO^{2+} \rightarrow FeOH^{2+} + O_2$ | $2.0 \times 10^6$ | | j |
| 136 | $OH + FeO^{2+} \xrightarrow{H_2O} FeOH^{2+} + H_2O_2$ | $1.0 \times 10^7$ | | j |
| 137 | $FeO^{2+} + H_2O \rightarrow FeOH^{2+} + OH$ | $1.3 \times 10^{-2}$ | 4100 | j |
| 138 | $FeO^{2+} + Fe^{2+} \xrightarrow{H_2O} 2\,FeOH^{2+}$ | $7.2 \times 10^4$ | 840 | j |
| 139 | $FeO^{2+} + Fe^{2+} \xrightarrow{H_2O} Fe(OH)_2Fe^{4+}$ | $1.8 \times 10^4$ | 5050 | j |
| 140 | $Fe(OH)_2Fe^{4+} \rightarrow 2\,FeOH^{2+}$ | 0.49 | 8800 | j |
| 141 | $HNO_2 + FeO^{2+} \rightarrow FeOH^{2+} + NO_2$ | $1.1 \times 10^4$ | 4150 | j |
| 142 | $NO_2^- + FeO^{2+} \xrightarrow{H^+} FeOH^{2+} + NO_2$ | $1.0 \times 10^5$ | | j |
| 143 | $HSO_3^- + FeO^{2+} \rightarrow FeOH^{2+} + SO_3^-$ | $2.5 \times 10^5$ | | j |
| 144 | $HCOOH + FeO^{2+} \xrightarrow{O_2} FeOH^{2+} + CO_2 + HO_2$ | 160 | 2680 | j |
| 145 | $HCOO^- + FeO^{2+} \xrightarrow{H^+,O_2} FeOH^{2+} + CO_2 + HO_2$ | $3.0 \times 10^5$ | | j |
| 146 | $FeOH^{2+} + HSO_3^- \rightarrow FeSO_3^+ + H_2O$ | $4.0 \times 10^6$ | | i |
| 147 | $FeSO_3^+ + H^+ \xrightarrow{OH^-} FeOH^{2+} + HSO_3^-$ | $2.08 \times 10^3$ | | i |
| 148 | $FeSO_3^+ \rightarrow Fe^{2+} + SO_3^-$ | 0.19 | | i |
| 149 | $Fe^{2+} + SO_3^- \rightarrow FeSO_3^+$ | $3.0 \times 10^6$ | 5605 | i |
| 150 | $FeOH^{2+} + SO_3^- \rightarrow Fe^{2+} + HSO_4^-$ | $3.0 \times 10^5 + 7.6 \times 10^6 \times 1.64 \times 10^{-3}\,[H^+]^{-1}$ | | i |
| 151 | $OH + Fe^{2+} \rightarrow FeOH^{2+}$ | $4.3 \times 10^8$ | 1100 | a |
| 152 | $H_2O_2 + FeOH^{2+} \rightarrow HO_2 + H_2O + Fe^{2+}$ | $2 \times 10^{-3}$ | | a |
| 153 | $O_2^- + FeOH^{2+} \rightarrow O_2 + Fe^{2+} + OH^-$ | $1.5 \times 10^8$ | | a |
| 154 | $HO_2 + FeOH^{2+} \rightarrow Fe^{2+} + O_2 + H_2O$ | $1.3 \times 10^5$ | | a |
| 155 | $O_2^- + Fe^{2+} \xrightarrow{H^+,H_2O} H_2O_2 + FeOH^{2+}$ | $1.0 \times 10^7$ | | a |
| 156 | $HO_2 + Fe^{2+} \xrightarrow{H_2O} H_2O_2 + FeOH^{2+}$ | $1.2 \times 10^6$ | 5050 | a |
| 157 | $NO_3 + Fe^{2+} \xrightarrow{OH^-} NO_3^- + FeOH^{2+}$ | $8 \times 10^6$ | | a |

| 158 | $FeOH^{2+} + HSO_3^- \rightarrow Fe^{2+} + SO_3^- + H_2O$ | 39 | | a |
|---|---|---|---|---|
| 159 | $Fe^{2+} + SO_5^- \xrightarrow{H_2O} FeOH^{2+} + HSO_5^-$ | $4.3 \times 10^7$ | | a |
| 160 | $Fe^{2+} + HSO_5^- \rightarrow FeOH^{2+} + SO_4^-$ | $3 \times 10^4$ | | a |
| 161 | $Fe^{2+} + SO_4^- \xrightarrow{H_2O} FeOH^{2+} + SO_4^{2-} + H^+$ | $3.5 \times 10^7$ | | a |
| 162 | $Fe^{2+} + S_2O_8^{2-} \xrightarrow{H_2O} FeOH^{2+} + SO_4^{2-} + SO_4^- + H^+$ | 17 | | a |
| 163 | $SO_4^- + Fe^{2+} \rightarrow FeSO_4^+$ | $3 \times 10^8$ | | a |
| 164 | $FeOH^{2+} + SO4^{2-} \rightarrow FeSO_4^+ + OH^-$ | $3.2 \times 10^3$ | | a |
| 165 | $FeSO_4^+ \xrightarrow{OH^-} FeOH^{2+} + SO_4^{2-}$ | $1.8 \times 10^5$ | | a |
| 166 | $Fe^{2+} + O_2 \xrightarrow{OH^-} FeOH^{2+} + O_2^-$ | $8.8 \times 10^{-2}$ | | e |
| 167 | $Fe^{2+} + O_2^- \xrightarrow{OH^-} FeOH^{2+} + O_2^{2-}$ | $10^7$ | | e |
| 168 | $O_2^- + FeSO_4^+ \rightarrow Fe^{2+} + SO_4^{2-} + O_2$ | $1.5 \times 10^{8\ b}$ | | g |
| 169 | $HO_2 + FeSO_4^+ \rightarrow Fe^{2+} + SO_4^{2-} + O_2 + H^+$ | $1.0 \times 10^3$ | | g |
| 170 | $Fe^{2+} + H_2O_2 \rightarrow FeO^{2+} + H_2O$ | See ref. | | k |
| | | | | |
| | **N-chemistry** | | | |
| 171 | $NO_2^- \xrightarrow{H^+,h\nu} NO + OH$ | See ref. | | f |
| 172 | $NO_3 \xrightarrow{H^+,h\nu} NO_2 + OH$ | See ref. | | f |
| 173 | $N_2O_5 + H_2O \rightarrow 2 H^+ + 2 NO_3^-$ | $5 \times 10^9$ | | a |
| 174 | $NO_3 + OH^- \rightarrow NO_3^- + OH$ | $9.4 \times 10^7$ | 2700 | a |
| 175 | $NO_3 + H_2O_2 \rightarrow NO_3^- + H^+ + HO_2$ | $4.9 \times 10^6$ | 2000 | a |
| 176 | $NO_3 + HSO_3^- \rightarrow NO_3^- + H^+ + SO_3^-$ | $1.3 \times 10^9$ | 2000 | a |
| 177 | $NO_3 + SO_3^{2-} \rightarrow NO_3^- + SO_3^-$ | $3.0 \times 10^8$ | | a |
| 178 | $NO_3 + HSO_4^- \rightarrow NO_3^- + H^+ + SO_4^-$ | $2.6 \times 10^5$ | | a |
| 179 | $NO_3 + SO_4^{2-} \rightarrow NO_3^- + SO_4^-$ | $5.6 \times 10^3$ | | a |
| 180 | $NO_2 + OH \rightarrow NO_3^- + H^+$ | $1.2 \times 10^{10}$ | | a |
| 181 | $NO_2 + O_2^- \rightarrow NO_2^- + O_2$ | $1 \times 10^8$ | | a |
| 182 | $NO_2 + NO_2 \xrightarrow{H_2O} HNO_2 + NO_3^- + H^+$ | $8.4 \times 10^7$ | -2900 | a |
| 183 | $O_2NO_2^- \rightarrow NO_2^- + O_2$ | $4.5 \times 10^{-2}$ | | a |
| 184 | $NO_2^- + NO_3 \rightarrow NO_3^- + NO_2$ | $1.4 \times 10^9$ | 0 | a |
| 185 | $SO_4^- + NO_3^- \rightarrow SO_4^{2-} + NO_3$ | $5.0 \times 10^4$ | | a |
| 186 | $HCOOH + NO_3 \xrightarrow{O_2} NO_3^- + H^+ + HO_2 + CO_2$ | $3.8 \times 10^5$ | 3400 | a |
| 187 | $HCOO^- + NO_3 \xrightarrow{O_2} NO_3^- + HO_2 + CO_2$ | $5.1 \times 10^7$ | 2200 | a |
| 188 | $NO_2 + HO_2 \rightarrow HO_2NO_2$ | $1.0 \times 10^7$ | | a |
| 189 | $HO_2NO_2 \rightarrow NO_2 + HO_2$ | $4.6 \times 10^{-3}$ | | a |
| 190 | $SO_4^- + NO_2^- \rightarrow SO_4^{2-} + NO_2$ | $9.8 \times 10^8$ | 1500 | b |
| 191 | $NO + NO_2 \xrightarrow{H_2O} 2 NO_2^- + 2 H^+$ | $2.0 \times 10^8$ | 1500 | c |
| 192 | $NO + OH \rightarrow NO_2^- + H^+$ | $2.0 \times 10^{10}$ | 1500 | c |
| 193 | $HNO_2 + OH \rightarrow NO_2 + H_2O$ | $1.0 \times 10^9$ | 1500 | c |
| 194 | $NO_2^- + OH \rightarrow NO_2 + OH^-$ | $1.0 \times 10^{10}$ | 1500 | c |
| 195 | $HNO_2 + H_2O_2 \xrightarrow{H^+} NO_3^- + 2 H^+ + H_2O$ | $6.3 \times 10^3 [H^+]$ | 6693 | c |
| 196 | $NO_2^- + O_3 \rightarrow NO_3^- + O_2$ | $5.0 \times 10^5$ | 6950 | c |
| 197 | $NO_3 + HO_2 \rightarrow NO_3^- + H^+ + O_2$ | $4.5 \times 10^9$ | 1500 | c |
| 198 | $NO_3 + O_2^- \rightarrow NO_3^- + O_2$ | $1.0 \times 10^9$ | 1500 | c |
| 199 | $2 NO_2 + HSO_3^- \xrightarrow{H_2O} SO_4^{2-} + 3 H^+ + 2 NO_2^-$ | $2.0 \times 10^6$ | 0 | l |
| 200 | $NO_2 + NO_2 \rightarrow N_2O_4$ | $4.5 \times 10^{8\ b}$ | | m |
| 201 | $N_2O_4 \xrightarrow{H_2O} 2 H^+ + NO_2^- + NO_3^-$ | $1.0 \times 10^{3\ b}$ | | m |
| 202 | $NO_3 + H_2O \rightarrow NO_3^- + OH + H^+$ | 6.0 | 4500 | n |

| 203 | $NO_3^- + OH + H^+ \rightarrow NO_3 + H_2O$ | $1.4 \times 10^8$ | | o |
| 204 | $HSO_5^- + NO_2^- \rightarrow HSO_4^- + NO_3^-$ | 0.31 | 6646 | p |
| | Carbonate chemistry | | | |
| 205 | $HCO_3^- + O_2^- \rightarrow HO_2^- + CO_3^-$ | $1.5 \times 10^6$ | 0 | c |
| 206 | $CO_3^- + H_2O_2 \rightarrow HO_2 + HCO_3^-$ | $8.0 \times 10^5$ | 2820 | c |
| 207 | $CO_2^- + O_2 \rightarrow O_2^- + CO_2$ | $2.4 \times 10^9$ | | q |
| 208 | $CO_3^- + O_2^- \rightarrow CO_3^{2-} + O_2$ | $6.8 \times 10^8$ | | q |
| 209 | $CO_3^- + HCOO^- \rightarrow HCO_3^- + CO_2^-$ | $1.5 \times 10^5$ | | q |
| 210 | $HCO_3^- + OH \rightarrow H_2O + CO_3^-$ | $1.7 \times 10^7$ | 1900 | a |
| 211 | $CO_3^{2-} + OH \rightarrow OH^- + CO_3^-$ | $3.9 \times 10^8$ | 2840 | a |
| 212 | $CO_3^{2-} + OH \rightarrow OH^- + CO_3^-$ | $4.1 \times 10^7$ | | a |
| 213 | $HCO_3^- + SO_4^- \rightarrow SO_4^{2-} + CO_3^- + H^+$ | $2.8 \times 10^6$ | 2090 | a |
| 214 | $CO_3^{2-} + NO_3 \rightarrow NO_3^- + CO_3^-$ | $4.1 \times 10^7$ | | a |
| 215 | $CO_3^- + CO_3^- \xrightarrow{O_2} 2\ O_2^- + 2\ CO_2$ | $2.2 \times 10^6$ | | a |
| 216 | $CO_3^- + Fe^{2+} \xrightarrow{OH^-} CO_3^{2-} + FeOH^{2+}$ | $2 \times 10^7$ | | a |
| 217 | $CO_3^- + HO_2 \rightarrow HCO_3^- + O_2$ | $6.5 \times 10^8$ | | a |
| 218 | $CO_3^- + HSO_3^- \rightarrow HCO_3^- + SO_3^-$ | $1 \times 10^7$ | | a |
| 219 | $CO_3^- + SO_3^{2-} \rightarrow CO_3^{2-} + SO_3^-$ | $5.0 \times 10^6$ | 470 | a |

170    [a] n = reaction order – 1. The units are s$^{-1}$ for first-order reactions and M$^{-1}$ s$^{-1}$ for second-order reactions. Reaction rate constant $k = k_{298} exp(-\frac{E_a}{R}(\frac{1}{T} - \frac{1}{298}))$.

[b] The temperature for k is 293 K.

References: a.(Herrmann et al., 2000), b.(Liang and Jacobson, 1999), c.(Seinfeld and Pandis, 2006), d.(Ponche et al., 1993), e.(Gonzalez et al., 2017), f.(Zellner et al., 1990), g.(Mao et al., 2013), h.(Matthijsen et al., 1995), i.(Warneck, 2018), j.(Deguillaume et al., 2005), k.(Tong
175   et al., 2017), l.(Lee and Schwartz, 1982), m.(Graedel and Weschler, 1981), n.(Jacob, 2000), o.(Rudich et al., 1996), p.(Jacob, 1986), q.(Liu et al., 2012a).

There are four parameters in every pair of gas-aqueous phase transfer equilibria. The two parameters in the transfer from the gas phase to the aqueous phase are the molar mass (g mol$^{-1}$) and mass accommodation coefficients of this species. The other

180   two parameters in the transfer from the aqueous phase to the gas phase are Henry's law constants at 298 K ($K_{H298}$) and $\Delta H/(500R)$, where $\Delta H$ (J mol$^{-1}$) is the enthalpy of dissolution and R is the ideal gas constant. "500" is the coefficient extracted from all $k_2$ for a more concise expression and "500 $k_2 = \Delta H/R$". The Henry's law constant $K_H$ (M atm$^{-1}$) at any temperature T (K) in Eq. (1) can be calculated by Eq. (2):

$$[C_i] = K_H \cdot P_i \tag{1}$$

185    $$K_H(T) = K_{H298} \cdot exp\left(-\frac{\Delta H}{R}\left(\frac{1}{T} - \frac{1}{298}\right)\right) \tag{2}$$

where $[C_i]$ and $P_i$ are aqueous-phase and gas-phase concentrations of species i in units of mol L$_{water}^{-1}$ and atm, respectively. On the other hand, the concentration of liquid water is a constant value of 55.6 (i.e., 1000/18) mol L$^{-1}$. The initial concentration of soluble Fe(III) ($[Fe^{3+}]$) is set to 5 μM, which refers to the urban conditions from the literature below (Deguillaume et al., 2005;Mao et al., 2013;Jacob, 2000;Shao et al., 2019;Li et al., 2017;Herrmann et al., 2000;Matthijsen et al., 1995).

190     To facilitate the calculation of gas-phase and aqueous-phase chemistry simultaneously, the methods used in Jacob (1986) and

Liu et al. (2012a) are applied in this study, which convert the units of concentrations and reaction rates in the aqueous phase

to the same units as those used in gas-phase chemistry (Jacob, 1986;Liu et al., 2012a):

$$[X_i] = 6.023 \times 10^{20} \cdot LWC \cdot [C_i] \tag{3}$$

where $[X_i]$ and $[C_i]$ are aqueous-phase concentrations of species i in units of molecules $cm_{air}^{-3}$ and mol $L_{water}^{-1}$, respectively,

195     and $6.023 \times 10^{20}$ is the product of Avogadro Constant ($6.023 \times 10^{23}$) and unit conversion factor ($10^{-3}$) between $L_{air}^{-1}$ and $cm_{air}^{-3}$.

In this way, the chemical systems of both gas and aqueous phases can be numerically solved without distinction.

### 2.3    Model configuration

Two main simulations are conducted in this study. The first simulation (the Original case) is conducted without any

modification of the default CAM4 chemistry, with parameterized aqueous-phase oxidation reactions of $SO_2$ by $H_2O_2$ and $O_3$.

200     In the second simulation (the Improved case), since the $F_{cld}$ is nonzero in most grids, two calculations are performed in a cloudy

grid cell. In the cloudy part, the parameterized aqueous-phase reactions mentioned above are replaced by detailed in-cloud

aqueous-phase chemistry listed in Tables 1a and 1b coupled with default gas chemistry. In the non-cloudy part, the calculation

is similar to the Original case but still without parameterized aqueous-phase reactions. Finally, the concentration in each grid

is the average of the cloudy and non-cloudy results weighted by $F_{cld}$.

205     The timestep used in this study is the default 30 minutes in CESM2. The lifetime of clouds (i.e., the time between the formation

and evaporation of clouds) is set equal to the timestep. At t = 0 of each step, all the cloud droplets are assumed to be

instantaneously and simultaneously formed, and all the water-soluble species (listed in Table 1a) are dissolved into the cloud

droplets according to the effective Henry's law constants. The pH value of each grid cell is calculated by the ionization

equilibria of ionizable species (listed in Table 1b) and the dissociation of CCN (including sulfate, nitrate and ammonium),

210     assuming that equilibrium and electroneutrality are continuously maintained. When t = 30 minutes, all the cloud droplets

instantaneously and simultaneously evaporate. All the species remaining in the aqueous phase are transferred directly back to

the gas phase. Low-volatility species such as ammonium, sulfate and nitrate are released directly back to the atmosphere as

inorganic aerosols.

On the basis of the Improved case, more sensitivity cases are simulated to explore the influences of different factors (e.g., the

215     concentration of soluble Fe and the pH value) on the capacity for $SO_2$ oxidation. The process of all these simulations is the

same as that of the Improved case.

Finally, all the simulations are performed for 2 years from 1 January 2014 to 31 December 2015. The first year is used for

model spin-up (Xu et al., 2019;Yi et al., 2017). The output of the simulation is in the form of a daily mean and is then converted

to a monthly or seasonal mean for research needs.

**2.4 Observations for evaluation of global simulation**

For the model evaluation, the observational data used in this study are collected from four monitoring networks. The observations in Europe (EU) are obtained from the European Monitoring and Evaluation Programme (EMEP, https://www.emep.int/, last access: 8 August 2020). The observations in the United States (US) are obtained from the U.S. Environmental Protection Agency Air Quality System (EPA, https://aqs.epa.gov/aqsweb/airdata/download_files.html#Raw, last access: 19 July 2020 ). The observations in China (CN) are obtained from the China National Environmental Monitoring Center (CNEMC, https://quotsoft.net/air/, last access: 22 December 2020). The observations in Japan and South Korea (JK) are obtained from the Acid Deposition Monitoring Network in East Asia (EANET, https://monitoring.eanet.asia/document/public/index, last access: 2 November 2020). The locations of monitoring stations are shown in Fig. 1. All observational data were collected from 1 January 2015 to 31 December 2015. The monthly averages used for analysis of the results are calculated from raw daily averages or even hourly averages collected from the measurement networks above. For convenience of comparison, the units of simulated concentration of $SO_2$ are all converted to the forms in corresponding observational data.
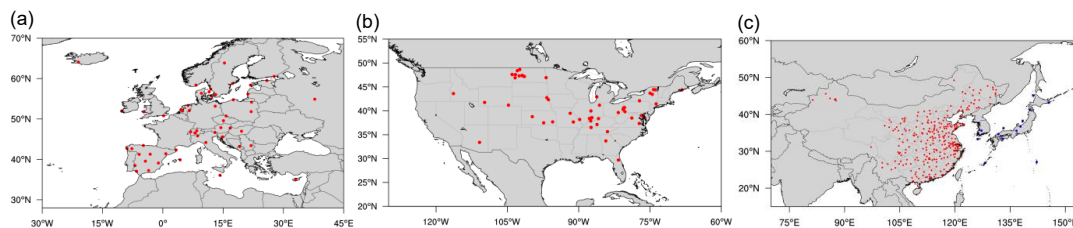
**Figure 1: Locations of monitoring sites from various measurement networks in (a) EU (EMEP), (b) US (EPA) and (c) EA (red points for CNEMC and blue points for EANET).**

**3 Effects of in-cloud aqueous-phase chemical mechanisms on the simulation of $SO_2$**

**3.1 Simulation of $SO_2$ in the Original case**

Figure 2 shows the seasonally averaged surface concentrations of $SO_2$ in the Original simulation. There are huge spatial and temporal differences in the global distribution of $SO_2$ concentrations. On the one hand, the concentrations of $SO_2$ are no more than 0.1 ppbv in most parts of the world and are basically concentrated in Asia, EU, North America (NA) and South Africa (SA), especially in Central and East CN. The concentrations in NA and EU are mainly in the ranges of 0.1-5 and 1-10 ppbv, respectively. The concentrations in EU are slightly higher than those in NA. Meanwhile, the concentration in the eastern US is evidently higher than that in the western US. In EA, the concentrations in JK range from 0.1 to 5 ppbv throughout the year. The concentrations in most of Central and East CN are in the range of 10-50 ppbv and even higher than 50 ppbv in some regions, which are much higher than those in other regions. In addition, similar to the US, the concentrations in Central and

East CN are much higher than that in Western CN. Such distributions are directly related to the high emissions of $SO_2$ in these regions of CN (Jo et al., 2020;Xie et al., 2016;Geng et al., 2019).

On the other hand, the concentrations of $SO_2$ are remarkably different in the four seasons. They are highest in winter, followed

250    by spring and autumn, and lowest in summer, especially in Asia and NA. Such seasonal differences are related to both emissions and the capacity for $SO_2$ oxidation in the gas phase. In winter, due to the increase in heating demand, the combustion of fossil fuels such as coal could significantly increase the emissions of $SO_2$ (Jo et al., 2020;Xie et al., 2016;Geng et al., 2019;Feng et al., 2020). At the same time, higher temperatures and stronger sunlight could enhance the gas-phase oxidation of $SO_2$ in summer, which is the opposite in winter. Such phenomena are consistent with multiple studies (Alexander et al.,

255    2009;Huang et al., 2014;Tilgner et al., 2013;Shao et al., 2019).
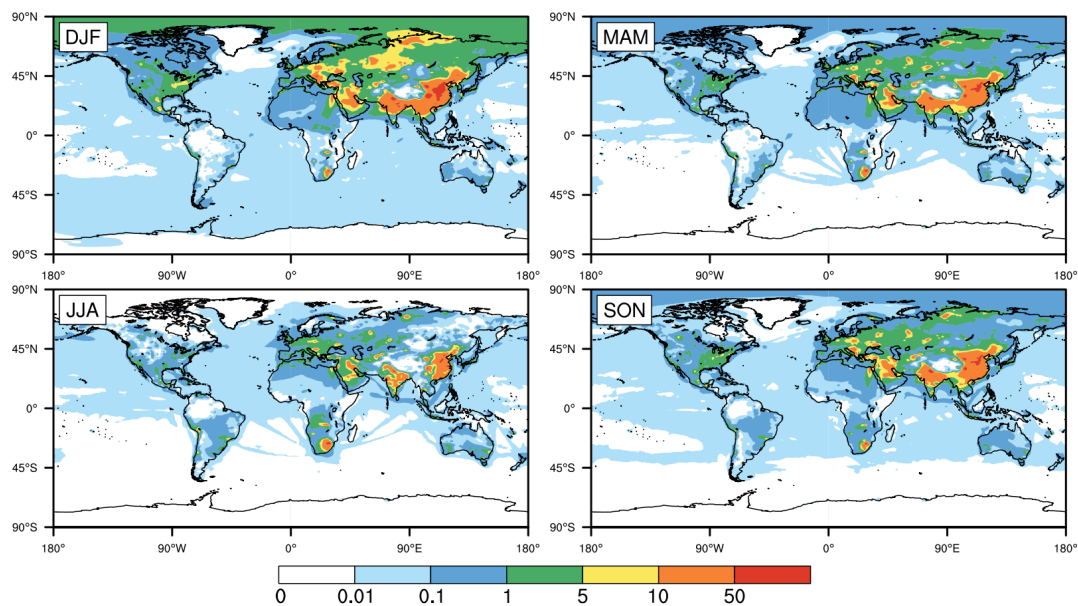
**Figure 2: Global distribution of seasonally averaged surface concentrations of $SO_2$ (ppbv) in 2015, simulated by CESM2 with standard configuration (i.e., the Original case). DJF, MAM, JJA and SON represent December-January-February, March-April-**

260    **May, June-July-August and September-October-November, respectively, the same below.**

### 3.2  Differences between the Original and Improved simulations

After replacement of default parameterized aqueous-phase reactions with detailed in-cloud aqueous-phase chemistry, the surface concentrations of $SO_2$ generally decrease markedly, as shown in Fig. 3. The extent of the reduction is distinct in different regions and seasons. In general, reductions in $SO_2$ mainly occur in Asia, EU, NA and SA. The concentrations of $SO_2$

265    decrease the most in CN, followed by EU, and the least in NA and JK. These results are partly due to the relatively high background concentrations in these regions in the Original simulation. Therefore, all the distribution patterns above are also similar to those in the Original simulation. The reductions in $SO_2$ also differs in various seasons. In NA and EU, the

concentrations of $SO_2$ in most regions are reduced by 0.1-5 and 1-10 ppbv in winter, respectively. In spring and autumn, the concentrations mainly decrease by 0.1-5 ppbv, which is slightly less than that in winter. However, the reduction in $SO_2$ in summer is very limited. Notably, the concentrations in some areas even increase slightly, which is partly due to the replacement of default parameterized aqueous-phase reactions. Sometimes these simplified and parameterized reactions are even stronger than detailed radical reactions, especially in summer. Similar to Fig. 2, Figure 3 shows that the decline in $SO_2$ concentrations in the eastern US is larger than that in the western US, which is also related to the background concentrations in the Original case. However, the situation is different in EA. The concentrations decrease significantly in all seasons in Central and East CN. The reduction is always more than 1 ppbv, sometimes even greater than 10 ppbv. Again, the reductions in Central and East CN are higher than that in Western CN. These results are also partly related to the background concentrations. The decrease in JK ranges from 0.1 to 5 ppbv throughout the year, without obvious fluctuation.
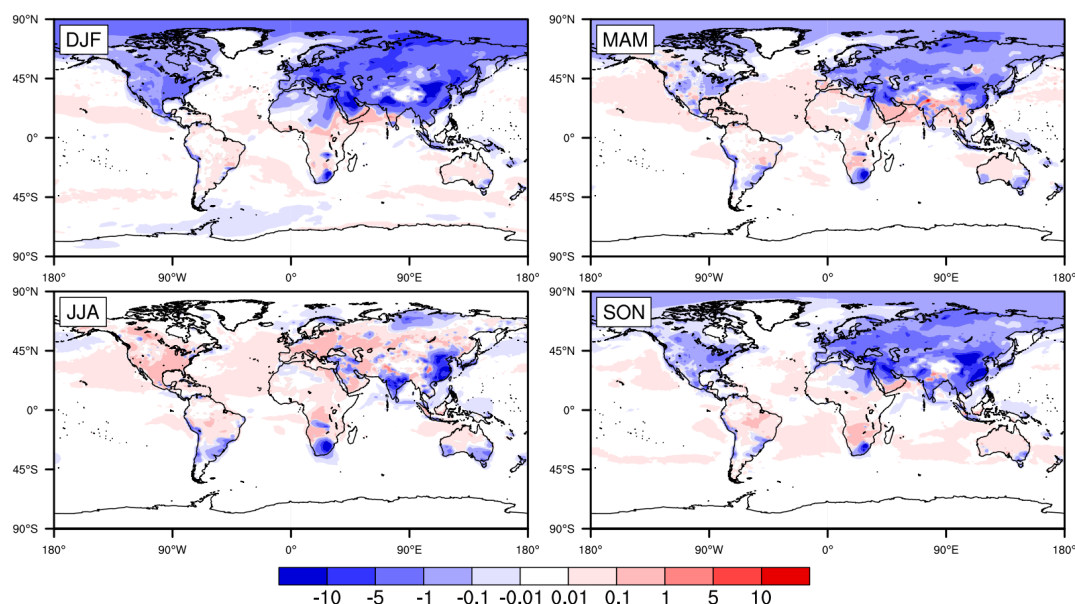
**Figure 3: The differences in global seasonally averaged surface $SO_2$ concentrations between the Improved case and the Original case in 2015 after the incorporation of detailed in-cloud aqueous-phase chemical mechanisms (ppbv).**

In regard to the relative differences between the Original and Improved cases, the results seem slightly different, as shown in Fig. S1 (see the supporting information). Although the reduction sequence is winter > autumn > spring > summer in general, which is very similar to the results above, the regional differences are no longer distinct. In winter, the concentrations of $SO_2$ decrease more than 50% in most regions of EU and NA but no more than 50% in Central and East CN. In contrast, the reductions are very small in EU, NA and JK in summer. However, the decreases exceed 10% in CN and even 50% in some regions (e.g., Shanxi, Hebei, Zhejiang and Fujian Provinces).

Such enhancement of the oxidation capacity can also be reflected in the net chemical loss rate of $SO_2$. Fig. S2 shows the ratio of the net chemical loss rates between the Improved and Original simulations. The net chemical loss rate increases in most

290 parts of the world (ratios > 1). The seasonal differences in the ratios are winter > autumn > spring > summer, which is still similar to the results above. The ratios in NA and JK are all more than 20 times greater and even above 100 times higher in some regions. Those in EU are more than 20 times greater in winter but less than 10 times higher in summer. The multiples in Western CN are all more than 20 times greater and even more than 100 times greater in some regions, which are much higher than those in East CN, which are only less than 10 times greater.

295 ## 3.3 Comparison between the simulated and observed $SO_2$ concentrations

The regional annual average concentrations between the simulated and observed $SO_2$ concentrations are summarized in Table 2. At the same time, scatter plots of $SO_2$ over various sites in the four monitoring networks are also shown in Fig. S3. Clearly, the effect of detailed aqueous-phase chemistry on the improvement in $SO_2$ simulation is remarkable. The annual average concentrations in the Original case are 4.3, 1.5, 2.0, and 1.6 times overestimated in EU, US, CN and JK, respectively. After

300 incorporating the detailed aqueous-phase chemistry, these values are reduced by 46%, 41%, 22% and 43%, respectively. The slopes of the linear fitting lines are all close to or even approximately equal to 1 in EU, US and JK.

**Table 2.** Comparison of regional annual average values among the Observed, Original-simulated and Improved-simulated $SO_2$ concentrations in EU, US, CN and JK in 2015. The observed concentrations are calculated by averaging the data from all monitoring

305 stations of various measurement networks. The simulated concentrations are calculated by averaging the data from all the grids where the monitoring stations are located.

| Region | Monitoring network | Units | Obs | Ori | Imp |
|---|---|---|---|---|---|
| EU | EMEP | µg S m$^{-3}$ | 0.51 | 2.7 | 1.4 |
| US | EPA | ppbv | 1.1 | 2.7 | 1.6 |
| CN | CNEMC | µg m$^{-3}$ | 27 | 82 | 63 |
| JK | EANET | ppbv | 0.54 | 1.38 | 0.78 |

The comparison between the simulated and observed monthly average concentrations of $SO_2$ in the four monitoring networks is shown in Fig. 4. The relative differences between the Original and Improved simulations are also shown in Fig. S4.

310 According to these two figures, compared with the observations, the Original simulation is generally overestimated in all regions, especially in winter. Coupling the detailed in-cloud aqueous-phase chemical mechanisms greatly improves the simulation of $SO_2$. In EU, aqueous-phase reactions significantly improve the simulation of $SO_2$ from October to February. The simulated concentrations decrease by more than 60% from the Original case to the Improved case and even by more than 75% in December. The Improved concentrations for six months are within the standard deviation of observations. The results in US

315 are even better than those in EU. The concentrations of $SO_2$ decrease more in winter, spring and autumn (-30 to -70%) than in

summer. All Improved concentrations are within the standard deviation of observations. Although the absolute reduction in SO₂ over CN is the greatest, the relative improvement in CN is the least due to the excessively high Original concentrations of SO₂. None of the simulated concentrations decrease by more than 40%. None of the Improved concentrations are within the standard deviation of observations. The aqueous-phase reactions also greatly improve the simulation in JK. The relative

320    differences in the four seasons are all close (approximately -30 to -60%). Almost all the Improved concentrations are also within the standard deviation of observations.
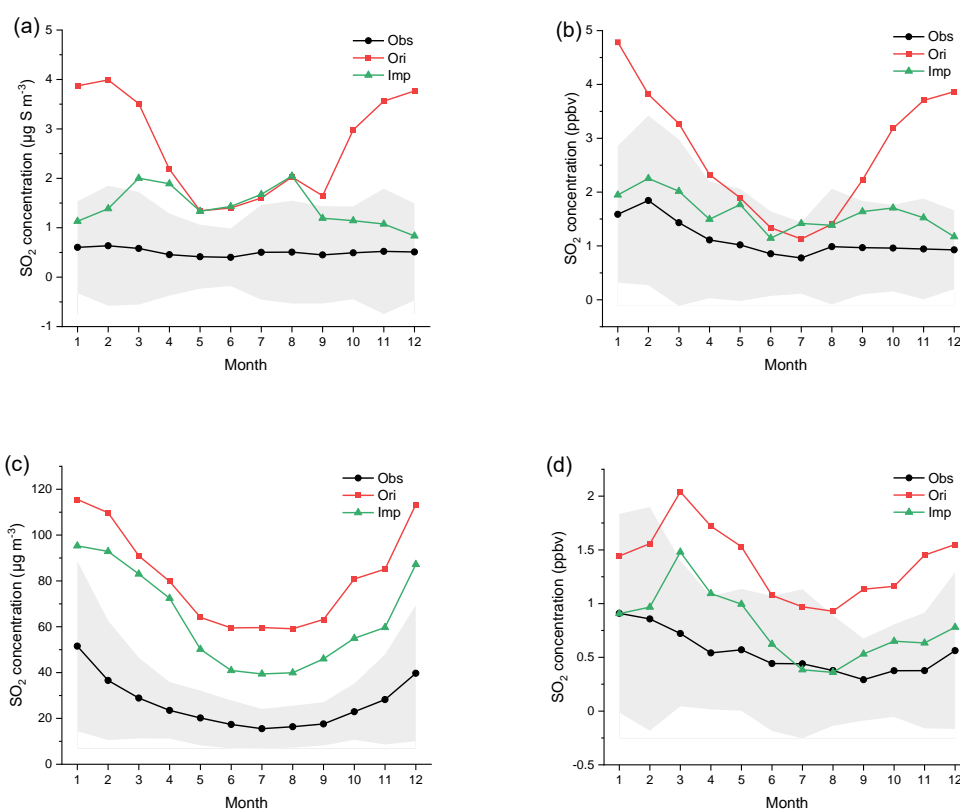
325    **Figure 4: Regional monthly average concentrations of SO₂ in EU, US, CN and JK in 2015. The black, red and green lines represent the Observed, Original-simulated and Improved-simulated concentrations, respectively. The gray areas represent the standard deviation of Observed concentrations. The corresponding monitoring networks are (a) EMEP (unit: µg S m⁻³), (b) EPA (unit: ppbv), (c) CNEMC (unit: µg m⁻³) and (d) EANET (unit: ppbv).**

Overall, the overestimation in winter is more serious than that in summer. At the same time, the improvement from adding

330    aqueous-phase chemistry is much greater in winter than in summer, especially in EU and US. These results indicate the importance of incorporating detailed aqueous-phase chemistry in winter and are highly consistent with the results of some existing studies (Shao et al., 2019;Ma et al., 2018;Huang et al., 2019). Such seasonal differences may be related to the ambient

temperature, humidity, and especially sunlight. In summer, both the temperature and sunlight are sufficient to generate a high concentration of ·OH (Lakey et al., 2016). Therefore, gas-phase oxidation is strong and dominant (Cheng et al., 2016).

335 However, due to the weak sunlight in winter, the gas-phase concentration of ·OH is two or three orders of magnitude less than that in summer. In addition, the rate constant is also less than 1/3-1/2 of that in summer owing to the decrease in temperature. Therefore, the gas-phase photochemical oxidation of $SO_2$ induced by ·OH is sharply weakened. These changes indicate the greatly increased importance of aqueous-phase reactions (Elser et al., 2016;Ervens, 2015;Harris et al., 2013;Huang et al., 2018). At the same time, higher humidity and more cloud coverage can provide a more sufficient aqueous environment, which is also

340 beneficial to improve the performance of aqueous-phase reactions, such as those that occur during winter in EU and US and summer in EA.

## 4    Contributions of different aqueous-phase chemical mechanisms to the oxidation of $SO_2$

On the basis of the above analysis of the overall detailed aqueous-phase chemistry, it is necessary to discuss the contributions of different aqueous-phase chemical mechanisms in detail. Figure 5 shows the effects of $HO_x$-chemistry, Fe-chemistry, N-

345 chemistry and carbonate chemistry on surface $SO_2$. Remarkable differences are clearly seen among these four mechanisms. On the one hand, generally speaking, the contributions from both $HO_x$-chemistry and Fe-chemistry to the oxidation of $SO_2$ are significant. Nonetheless, the seasonal and regional distribution properties of these two chemical mechanisms are obviously different. For $HO_x$-chemistry, the concentrations of $SO_2$ decrease in most parts of the world, and the seasonal differences are very small. The reductions generally range from 0.01-0.1 ppbv over the ocean and 0.1-5 ppbv over land. In regard to Fe-

350 chemistry, however, the reduction in $SO_2$ is mostly concentrated on land only, especially in the Northern Hemisphere. The seasonal properties of the reductions are nearly the same as those described in Sect. 3.2. On the other hand, these two chemical mechanisms contribute much more than N-chemistry to the oxidation of $SO_2$. The decrease in $SO_2$ exceeds 1 ppbv in many regions of Asia, EU and NA due to the effects of Fe-chemistry or $HO_x$-chemistry. Meanwhile, the contribution of N-chemistry almost never exceeds 1 ppbv. Such great disparity may be related to the level of Fe concentrations and pH values in cloud

355 water, which are discussed in Sect. 5. In regard to carbonate chemistry, however, it is difficult to see a consistent spatial or temporal trend. The concentration of $SO_2$ decreases in some places and seasons but increases in other places and seasons. Moreover, all the changes are very small, within ±0.1 ppbv. Therefore, carbonate chemistry has no significant effect on the oxidation of $SO_2$.
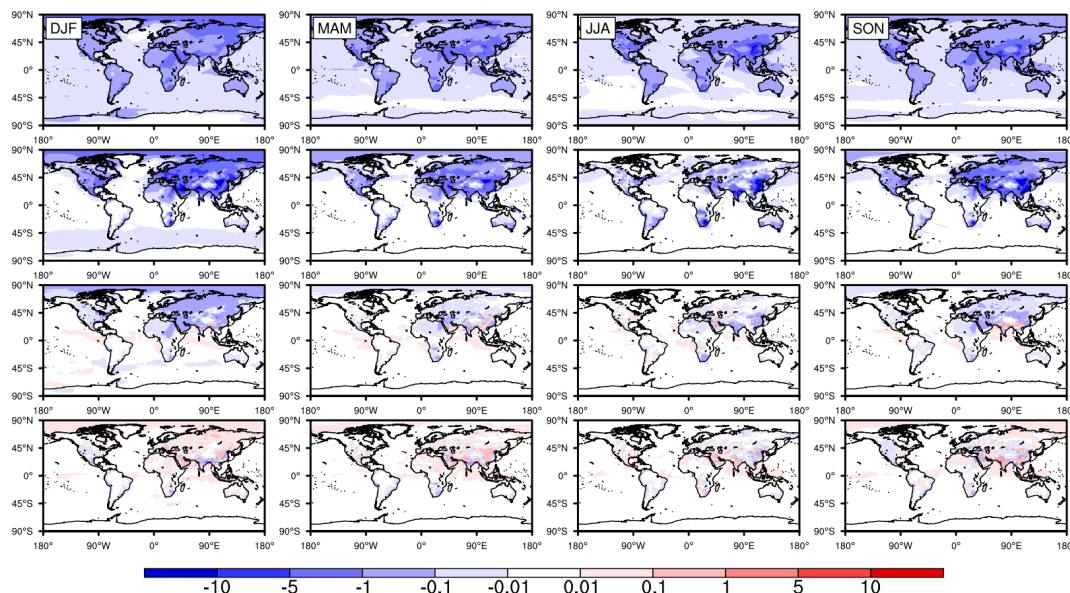
**Figure 5: The differences in global seasonally averaged surface SO₂ concentrations (ppbv) in 2015 with the incorporation of HO$_x$-chemistry, Fe-chemistry, N-chemistry and carbonate chemistry individually from top to bottom, respectively.**

The contributions of the different chemical mechanisms discussed above can also be seen from the relative differences, as shown in Fig. S5. HO$_x$-chemistry contributes the most over the ocean in the Southern Hemisphere. At the same time, Fe-chemistry contributes the most over land in the Northern Hemisphere. The concentrations of SO₂ decrease by more than 50% by both mechanisms. Furthermore, note that although the contribution of carbonate chemistry is quite small, there is an evident decrease over the ocean in the Southern Hemisphere.

## 5    Factors affecting the capacity for SO₂ oxidation from aqueous-phase reactions

### 5.1    The concentration of soluble Fe

The concentrations of soluble $[Fe^{3+}]$ are all set to 5 μM in the Improved case. Nevertheless, $[Fe^{3+}]$ varies greatly in different regions, seasons and ambient conditions. For instance, $[Fe^{3+}]$ is generally no more than 0.1 μM under marine conditions and no more than 1 μM under remote continental conditions (Herrmann et al., 2000;Matthijsen et al., 1995;Deguillaume et al., 2005;Mao et al., 2013;Jacob, 2000;Shao et al., 2019;Li et al., 2017). In many polluted cities, $[Fe^{3+}]$ is much higher than that in remote regions, usually ranging from 5-20 μM and sometimes even exceeding 100 μM (Matthijsen et al., 1995;Deguillaume et al., 2005;Herrmann et al., 2000;Mao et al., 2013;Jacob, 2000;Li et al., 2017). Therefore, in this study, four other levels of $[Fe^{3+}]$ (0.1, 1, 20 and 100 μM) are added to evaluate the influence of soluble Fe concentration on the capacity for SO₂ oxidation with all of the aqueous-phase chemical mechanisms. All the levels of $[Fe^{3+}]$ are referred from the studies above.

The regional monthly average concentrations of $SO_2$ in four regions are shown in Fig. 6. In all four regions, the simulated $SO_2$

concentrations first still increase in summer when $[Fe^{3+}]$ is 0.1 μM and then decrease considerably when $[Fe^{3+}]$ increases from

380    0.1 μM to 5 μM but decline only slightly when $[Fe^{3+}]$ increases to 20 μM. The two lines of "[Fe] = 20 μM" and "[Fe] = 100

μM" almost overlap and cannot be distinguished clearly in EU, US and JK. Only in CN does the concentration of $SO_2$ further

decrease obviously when $[Fe^{3+}]$ increases from 5 μM to 100 μM. There are many steel and coal factories and power plants in

CN. These results imply that there may be a strong correlation between high emissions of $SO_2$ and iron and that the

concentrations of Fe in CN may be higher than those in other regions.

385
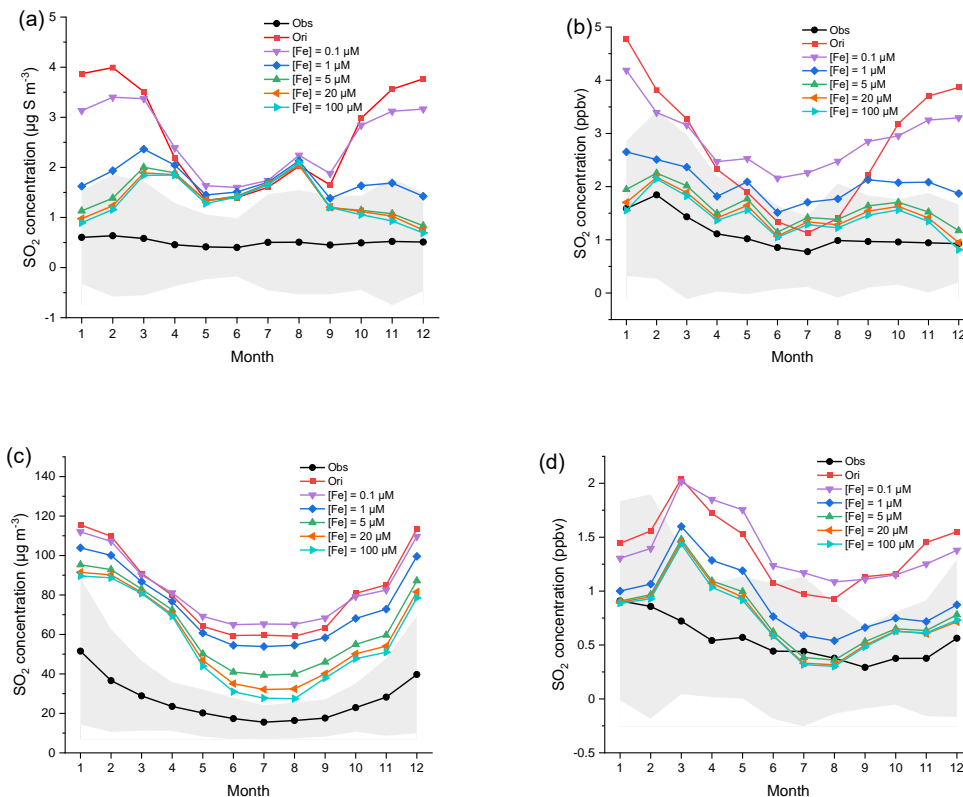
**Figure 6: Regional monthly average concentrations of $SO_2$ in EU, US, CN and JK in 2015. The black and red lines represent the Observed and Original-simulated concentrations of $SO_2$, respectively. Other lines represent $SO_2$ concentrations with different**

390    **soluble $[Fe^{3+}]$. $[Fe^{3+}]$ from top to bottom are 0.1, 1, 5 (i.e., the Improved case), 20 and 100 μM, respectively. The gray areas represent the standard deviation of Observed concentrations. The corresponding monitoring networks are (a) EMEP (unit: μg S m⁻³), (b) EPA (unit: ppbv), (c) CNEMC (unit: μg m⁻³) and (d) EANET (unit: ppbv).**

Such a trend in the capacity for $SO_2$ oxidation with $[Fe^{3+}]$ can also be seen in the global distributions in Fig. S6. The capacity

for $SO_2$ oxidation is enhanced with increasing $[Fe^{3+}]$ on the whole. When $[Fe^{3+}]$ is only 0.1 μM, the effect of Fe-chemistry is

395    still quite weak. The effect is rapidly enhanced when $[Fe^{3+}]$ increases from 0.1 μM to 5 μM. However, such enhancement

becomes markedly less when $[Fe^{3+}]$ is greater than 20 μM. The concentration of $SO_2$ is almost unchanged when $[Fe^{3+}]$ increases

to 100 μM. This result indicates that the effect of increasing $[Fe^{3+}]$ on the capacity for $SO_2$ oxidation has a threshold. Too much

$[Fe^{3+}]$ will not further facilitate the oxidation of $SO_2$. The reason for such a limitation is discussed below.

In any case, a higher concentration of soluble Fe results in an improvement in the $SO_2$ simulation compared to the observations.

400    **5.2   The pH value**

As mentioned in the Introduction, the pH value in cloud water is a key parameter for aqueous-phase chemistry, which could

directly affect ionization equilibria and gas-aqueous mass transfer processes. There are expressions for the rate constants of

several aqueous-phase reactions, and some expressions include pH values directly. Therefore, the pH value could affect the

various aqueous-phase reaction rates, especially that of N-chemistry (Shao et al., 2019;Li et al., 2017;Cheng et al., 2016;He et

405    al., 2018;He and He, 2020). Therefore, it is necessary to discuss the influence of the pH value on the capacity for $SO_2$ oxidation,

such as the monthly average concentrations shown in Fig. 7. In this study, there are four levels of pH value (3, 4, 5 and 6). All

the pH values are obtained from multiple studies (Herrmann et al., 2000;Matthijsen et al., 1995;Shao et al., 2019;Guo et al.,

2017;Cheng et al., 2016). $[Fe^{3+}]$ is set to 5 μM. However, it is difficult to see obvious differences among these four pH levels

in all seasons. Only a small decrease in $SO_2$ can be seen in most regions from pH 3 to 4. The reduction in $SO_2$ is almost the

410    same from pH 4 to 6. This result indicates that the effect of increasing the pH value on the capacity for $SO_2$ oxidation is limited.

The global distributions of $SO_2$ in different seasons shown in Fig. S7 have similar features. Although the capacity for $SO_2$

oxidation increases to some extent from pH 3 to 4 in all four regions, the changes from pH 4 to 6 are very small.

Notwithstanding, a higher pH value doubtless enhances the capacity for $SO_2$ oxidation and results in simulated values that are

closer to the observations, which is similar to the influence of the soluble Fe concentration (Shi et al., 2019;Shao et al., 2019;Li

415    et al., 2017;Cheng et al., 2016).

It seems that the influence of the pH value on the aqueous-phase chemistry is much weaker than that of the soluble Fe

concentration. When further discussing the effect of the pH value on N-chemistry, $HO_x$-chemistry or Fe-chemistry individually,

however, the situation is quite different, as shown in Figs. S8-10. When the pH increases from 3 to 6, the capacity for $SO_2$

oxidation from N-chemistry and $HO_x$-chemistry is evidently enhanced at all times. When the pH is 6, the oxidation capacity

420    from N-chemistry and $HO_x$-chemistry becomes almost as strong as that from Fe-chemistry with a high concentration of soluble

Fe. This indicates that the capacity for $SO_2$ oxidation from N-chemistry and $HO_x$-chemistry is greatly affected by the pH value

(Wang et al., 2020;Cheng et al., 2016;He et al., 2018;Li et al., 2018b;He and He, 2020). In contrast, the capacity for $SO_2$

oxidation from Fe-chemistry is the opposite. When $[Fe^{3+}]$ is set at the default medium level (5 μM), regardless of the pH, there

are no remarkable changes in $SO_2$ concentrations, and the capacity for $SO_2$ oxidation from Fe-chemistry is nearly the same,

425    especially when the pH ranges from 4 to 6. This indicates that the Fe-chemistry is not significantly affected by pH.
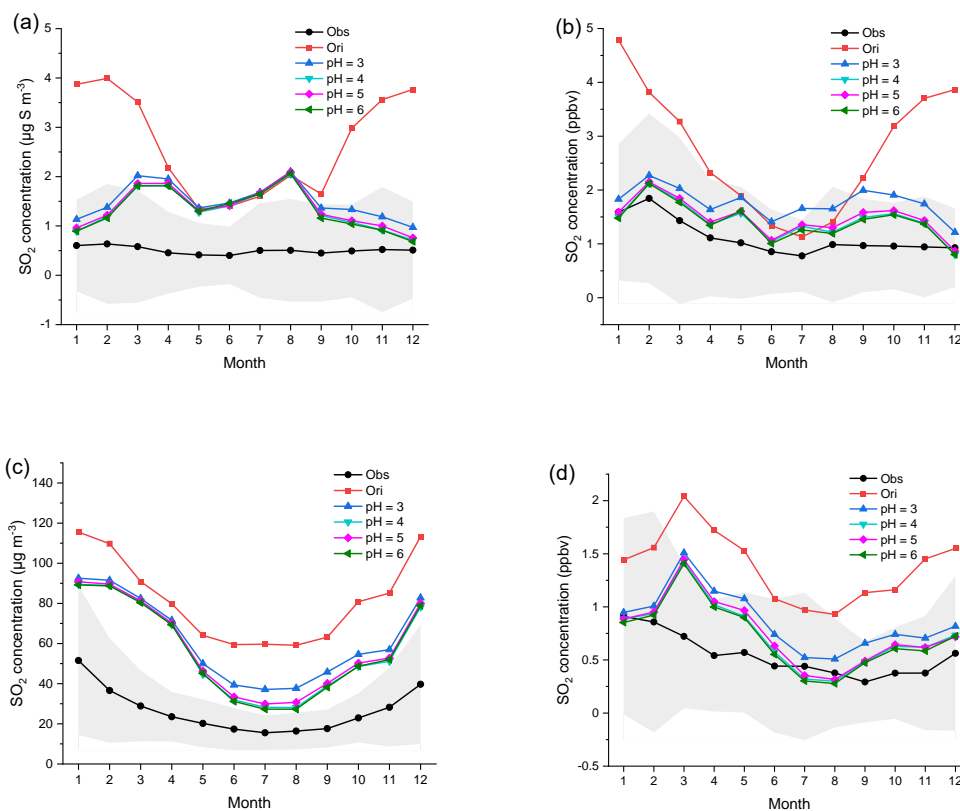
**Figure 7: Regional monthly average concentrations of SO₂ in EU, US, CN and JK in 2015. The black and red lines represent the**
**Observed and Original-simulated concentrations of SO₂, respectively. Other lines represent SO₂ concentrations at different pH**
**values. The pH values from top to bottom are 3, 4, 5 and 6, respectively. [Fe³⁺] is set to 5 µM. The gray areas represent the standard**
**deviation of Observed concentrations. The corresponding monitoring networks are (a) EMEP (unit: µg S m⁻³), (b) EPA (unit: ppbv),**
**(c) CNEMC (unit: µg m⁻³) and (d) EANET (unit: ppbv).**

These results well explain why the contribution of N-chemistry is much smaller than those of Fe-chemistry and HO$_x$-chemistry

in Sect. 4. According to the simulation, the pH value in cloud water is generally in the range of 3-5. This pH range is highly

consistent with those in previous studies (Herrmann et al., 2000;Matthijsen et al., 1995;Shao et al., 2019;Guo et al., 2017;Cheng

et al., 2016). As seen in Fig. 5, the capacity for SO$_2$ oxidation from N-chemistry is between pH 4 and 5, which is still not

strong enough. Consequently, the capacity for SO$_2$ oxidation from N-chemistry is largely limited by the relatively low pH

values in cloud water.

As analyzed in the sections above, it is worth noting that regardless of the high soluble Fe concentration or high pH value for

different chemical mechanisms, the reduction in SO$_2$ always seems to reach a very similar limitation, whose global distribution

and regional monthly average concentrations are also almost the same. This is not only related to soluble Fe concentration, pH

value or the chemical properties of various mechanisms themselves but also derived from the exhaustion of $SO_2(aq)$ by detailed aqueous-phase chemistry in a finite cloud. The aqueous-phase chemistry cannot affect regions without clouds because the total

445   concentration of $SO_2$ is calculated by weighted averages of "cloudy" and "non-cloudy" conditions according to $F_{cld}$. The overestimated $SO_2$ is sometimes caused by a shortage of clouds, especially in CN. Therefore, only more cloud coverage or lower emissions may further reduce the overestimation.

Consequently, it is easy to conclude that the oxidation capacity of Fe-chemistry and $HO_x$-chemistry is much higher than that of N-chemistry when the pH is less than 5, but evaluating their relative importance at high pH is difficult. The cloud content

450   and substrate concentration become the limiting factors. Therefore, a comprehensive investigation of cloud pH in different seasons and different places is urgently needed.

### 5.3   Uncertainty analysis

In addition to the soluble Fe concentration and pH value discussed above, there are some other factors that may also affect the capacity for $SO_2$ oxidation and increase the uncertainty of the simulation. First, the simulation of variables related to cloud

455   properties (such as LWC, $F_{cld}$ and r) directly determines the contribution of aqueous-phase chemistry. However, the simulation of these variables is also one of the greatest uncertainties (Zhang et al., 2019;Faloona, 2009). In addition, the initial valence of soluble Fe and the proportion of various valences are related to the capacity of Fe-chemistry. The higher the proportion of $Fe^{3+}$ is, the stronger the atmospheric oxidizability and the more helpful for the oxidation of $SO_2$ (Jacob, 2000;Deguillaume et al., 2005;Huang et al., 2014;Alexander et al., 2009). Moreover, the emissions and solubility of Fe vary greatly in different regions.

460   For instance, the total concentration of atmospheric Fe is generally measured in the range of 1-1000 ng $m_{air}^{-3}$, and the solubility of Fe varies from less than 1% to 10% (Cwiertny et al., 2008;Hsu et al., 2010;Sedwick et al., 2007;Sholkovitz et al., 2009;Hsu et al., 2013;Heal et al., 2005;Ingall et al., 2018;Mao et al., 2013;Itahashi et al., 2018;Shelley et al., 2018;McDaniel et al., 2019;Conway et al., 2019;Shi et al., 2020;Myriokefalitakis et al., 2018;Wang et al., 2015). Meanwhile, the simulated LWC usually ranges from $10^{-8}$ to $10^{-5}$ $L_{water}$ $L_{air}^{-1}$ in CESM2 and other model studies (Herrmann et al., 2000;Jacob, 1986;Matthijsen

465   et al., 1995;Liu et al., 2012a;Herrmann et al., 2015). In addition, $F_{cld}$ should also be considered. Therefore, the concentration of soluble Fe can be calculated to range from less than $10^{-3}$ μM to $10^3$ μM, which implies great uncertainty. At the same time, the proportions of aerosols containing sulfate, nitrate and ammonium in the aqueous phase could directly affect the pH of cloud water. The simulated pH value of cloud water itself is one of the sources of uncertainty (Shi et al., 2019;Xue et al., 2016). Finally, some sources of kinetic parameters for the aqueous-phase reactions are outdated. They may also not be accurate

470   enough because measurement conditions in the laboratory are different from the conditions of the real atmosphere. These issues influence the accuracy of the reaction rates and increase the uncertainty of the simulation.

In addition, there are factors that affect the performance of the simulation to a certain degree. First, an accurate emission inventory is the premise for improving the simulation (Im et al., 2018;de Meij et al., 2006;Liu et al., 2018;Buchard et al., 2014).

The data sources and resolutions of various emission types could affect the reliability of the inventory. For instance, regardless of how the parameters discussed above are optimized, the concentration of $SO_2$ in CN is always overestimated, which may be related to the uncertainties in emission inventories. The emissions of $SO_2$ in CN have decreased considerably in recent years, which may lead to biases in the simulations (Jo et al., 2020;Xie et al., 2016;Geng et al., 2019). Meanwhile, the meteorological data include information on the water content, wind, temperature and pressure, which all influence the formation and movements of clouds. Therefore, the reliability of meteorological data is also related to the uncertainty of simulations with in-cloud chemistry (Bei et al., 2017;Liu et al., 2007). At the same time, the simulation of the $SO_2$ wet deposition process also involves great uncertainty. Furthermore, the selection of monitoring stations determines the quality of observational data. As a global model, CESM2 used in this study has a resolution that is still not fine enough to accurately simulate regions that are too remote or too close to pollution sources. The simulation of each grid can represent only the average level of a region. Therefore, the monitoring stations should also represent the average level of the region. Otherwise, the limitation of the model resolution also increases the deviation of the comparison with observations and the uncertainty of the simulations. Finally, there are slight numerical fluctuations during the calculation of the model itself, but the uncertainty from the fluctuations is very small and can be ignored, especially after the results are averaged.

## 6    Conclusion

To improve the global simulation of $SO_2$, in this study, we used CESM2 to evaluate the effects of detailed in-cloud aqueous-phase reaction mechanisms on the capacity for $SO_2$ oxidation. After the replacement of default simplified and parameterized aqueous-phase reactions with detailed in-cloud aqueous-phase reactions, the overestimation of surface $SO_2$ concentrations generally decreases significantly. The reductions vary in different regions and seasons. Most them are in the range of 0.1-10 ppbv and some can be greater than 10 ppbv in some regions of CN. The net chemical loss rate of $SO_2$ also increases substantially. When compared with the observations, the simulated values that incorporate detailed aqueous-phase chemistry improve greatly, making the simulations much closer to the observations. The biases of annual average simulated concentrations decrease by 46%, 41%, 22% and 43% in EU, US, CN and JK, respectively. The concentration even decreases by approximately 70% in winter in EU, which is very close to the observed value. The concentrations of $SO_2$ in CN are still highly overestimated, although they decrease considerably. Aqueous-phase chemistry contributes more in EU, US and JK than in CN, which may be related to cloud coverage and emissions.

The contribution of each aqueous-phase mechanism to the simulation of $SO_2$ also differs significantly. Fe-chemistry and $HO_x$-chemistry contribute more to the capacity for $SO_2$ oxidation than N-chemistry. Carbonate chemistry has no significant effect on the oxidation of $SO_2$. Several factors could influence the capacity for $SO_2$ oxidation. Higher concentrations of soluble Fe and higher pH values could further enhance the oxidation capacity and improve the simulation of $SO_2$. In addition, the oxidation

capacities from N-chemistry and $HO_x$-chemistry are strongly affected by pH values and increase rapidly with increasing pH.

505    The oxidation capacity from Fe-chemistry is almost unaffected by pH. Many other factors also affect the aqueous-phase chemistry and the simulation of $SO_2$. Regardless of which factor changes, there is still a limitation on the improvement in the simulations because of limited cloud coverage in the aqueous phase.

This study emphasizes the importance of aqueous-phase chemical mechanisms for $SO_2$ oxidation. These mechanisms are helpful to improve the simulation of $SO_2$ by CESM2, deepening the understanding of $SO_2$ oxidation and the formation of

510    sulfate, $PM_{2.5}$ and even haze days. A better simulation of $SO_2$ is a prerequisite for better representing sulfate, which further influences cloud microphysics, radiation transfer and climate change.

However, some aspects still need to be further studied and improved in the future. For instance, there is a high degree of uncertainty in the concentration of soluble Fe owing to the dramatically large variation in the total atmospheric Fe content and Fe solubility in different regions. At the same time, there are few observational data or emission inventories of soluble Fe.

515    Therefore, the contribution of Fe-chemistry to the capacity for $SO_2$ oxidation is uncertain under different atmospheric conditions and difficult to evaluate accurately. Meanwhile, many variables and parameters related to the simulated clouds are also uncertain, such as LWC, $F_{cld}$, r, pH values in clouds, wet deposition processes, and proportions of inorganic aerosols in the aqueous phase. Therefore, it is urgently necessary to compare these variables with observational data if possible. Moreover, the effect of aqueous-phase chemistry on $SO_2$ at high altitude is not discussed in this study. These issues will be examined in

520    our future work.

**Code availability**

The Community Earth System Model 2(CESM2) developed by the National Center for Atmospheric Research can be downloaded online (https://www.cesm.ucar.edu/models/cesm2/). All codes used to generate the results of this study are available from the authors upon request.

525    **Data availability**

The CMIP6 emission datasets analyzed during the current study are available at https://svn-ccsm-inputdata.cgd.ucar.edu/trunk/inputdata/atm/cam/chem/. The MERRA2 meteorological offline data are publicly available from https://rda.ucar.edu/datasets/ds313.3/.

**Competing interests**

530    The authors declare that they have no conflict of interest.

**Acknowledgements**

This work was supported by funding from the National Natural Science Foundation of China (under award nos. 42077196, 41821005) as well as the Newton Advanced Fellowship (NAFR2180103).

**References**

535    Alexander, B., Park, R. J., Jacob, D. J., and Gong, S.: Transition metal-catalyzed oxidation of atmospheric sulfur: Global implications for the sulfur budget, Journal of Geophysical Research, 114, 10.1029/2008jd010486, 2009.

Au Yang, D., Bardoux, G., Assayag, N., Laskar, C., Widory, D., and Cartigny, P.: Atmospheric $SO_2$ oxidation by $NO_2$ plays no role in the mass independent sulfur isotope fractionation of urban aerosols, Atmospheric Environment, 193, 109-117, 10.1016/j.atmosenv.2018.09.007, 2018.

540    Bataineh, H., Pestovsky, O., and Bakac, A.: pH-induced mechanistic changeover from hydroxyl radicals to iron(iv) in the Fenton reaction, Chemical Science, 3, 10.1039/c2sc20099f, 2012.

Bei, N., Wu, J., Elser, M., Feng, T., Cao, J., El-Haddad, I., Li, X., Huang, R., Li, Z., Long, X., Xing, L., Zhao, S., Tie, X., Prévôt, A. S. H., and Li, G.: Impacts of meteorological uncertainties on the haze formation in Beijing–Tianjin–Hebei (BTH) during wintertime: a case study, Atmospheric Chemistry and Physics, 17, 14579-14591, 10.5194/acp-17-14579-2017, 2017.

545    Bell, N., Koch, D., and Shindell, D. T.: Impacts of chemistry-aerosol coupling on tropospheric ozone and sulfate simulations in a general circulation model, Journal of Geophysical Research: Atmospheres, 110, 10.1029/2004jd005538, 2005.

Bray, W. C., and Gorin, M. H.: Ferryl ion, a compound of tetravalent iron, J Am Chem Soc, 54, 2124-2125, DOI 10.1021/ja01344a505, 1932.

Buchard, V., da Silva, A. M., Colarco, P., Krotkov, N., Dickerson, R. R., Stehr, J. W., Mount, G., Spinei, E., Arkinson, H. L.,

550    and He, H.: Evaluation of GEOS-5 sulfur dioxide simulations during the Frostburg, MD 2010 field campaign, Atmospheric Chemistry and Physics, 14, 1929-1941, 10.5194/acp-14-1929-2014, 2014.

Chen, Y., Luo, X. S., Zhao, Z., Chen, Q., Wu, D., Sun, X., Wu, L., and Jin, L.: Summer-winter differences of $PM_{2.5}$ toxicity to human alveolar epithelial cells (A549) and the roles of transition metals, Ecotoxicol Environ Saf, 165, 505-509, 10.1016/j.ecoenv.2018.09.034, 2018.

555    Cheng, Y. F., Zheng, G. J., Wei, C., Mu, Q., Zheng, B., Wang, Z. B., Gao, M., Zhang, Q., He, K. B., Carmichael, G., Poschl, U., and Su, H.: Reactive nitrogen chemistry in aerosol water as a source of sulfate during haze events in China, Sci Adv, 2, ARTN e160153010.1126/sciadv.1601530, 2016.

Conway, T. M., Hamilton, D. S., Shelley, R. U., Aguilar-Islas, A. M., Landing, W. M., Mahowald, N. M., and John, S. G.: Tracing and constraining anthropogenic aerosol iron fluxes to the North Atlantic Ocean using iron isotopes, Nat Commun, 10,

560    2628, 10.1038/s41467-019-10457-w, 2019.

Cwiertny, D. M., Baltrusaitis, J., Hunter, G. J., Laskin, A., Scherer, M. M., and Grassian, V. H.: Characterization and acid-mobilization study of iron-containing mineral dust source materials, Journal of Geophysical Research: Atmospheres, 113, 10.1029/2007jd009332, 2008.

Danabasoglu, G., Lamarque, J. F., Bacmeister, J., Bailey, D. A., DuVivier, A. K., Edwards, J., Emmons, L. K., Fasullo, J.,
565   Garcia, R., Gettelman, A., Hannay, C., Holland, M. M., Large, W. G., Lauritzen, P. H., Lawrence, D. M., Lenaerts, J. T. M., Lindsay, K., Lipscomb, W. H., Mills, M. J., Neale, R., Oleson, K. W., Otto-Bliesner, B., Phillips, A. S., Sacks, W., Tilmes, S., Kampenhout, L., Vertenstein, M., Bertini, A., Dennis, J., Deser, C., Fischer, C., Fox-Kemper, B., Kay, J. E., Kinnison, D., Kushner, P. J., Larson, V. E., Long, M. C., Mickelson, S., Moore, J. K., Nienhouse, E., Polvani, L., Rasch, P. J., and Strand, W. G.: The Community Earth System Model Version 2 (CESM2), Journal of Advances in Modeling Earth Systems, 12,
570   10.1029/2019ms001916, 2020.

de Meij, A., Krol, M., Dentener, F., Vignati, E., Cuvelier, C., and Thunis, P.: The sensitivity of aerosol in Europe to two different emission inventories and temporal distribution of emissions, Atmospheric Chemistry and Physics, 6, 4287-4309, DOI 10.5194/acp-6-4287-2006, 2006.

Deguillaume, L., Leriche, M., and Chaumerliac, N.: Impact of radical versus non-radical pathway in the Fenton chemistry on
575   the iron redox cycle in clouds, Chemosphere, 60, 718-724, 10.1016/j.chemosphere.2005.03.052, 2005.

Elser, M., Huang, R.-J., Wolf, R., Slowik, J. G., Wang, Q., Canonaco, F., Li, G., Bozzetti, C., Daellenbach, K. R., Huang, Y., Zhang, R., Li, Z., Cao, J., Baltensperger, U., El-Haddad, I., and Prévôt, A. S. H.: New insights into $PM_{2.5}$; chemical composition and sources in two major cities in China during extreme haze events using aerosol mass spectrometry, Atmospheric Chemistry and Physics, 16, 3207-3225, 10.5194/acp-16-3207-2016, 2016.

580   Emmons, L. K., Walters, S., Hess, P. G., Lamarque, J. F., Pfister, G. G., Fillmore, D., Granier, C., Guenther, A., Kinnison, D., Laepple, T., Orlando, J., Tie, X., Tyndall, G., Wiedinmyer, C., Baughcum, S. L., and Kloster, S.: Description and evaluation of the Model for Ozone and Related chemical Tracers, version 4 (MOZART-4), Geoscientific Model Development, 3, 43-67, DOI 10.5194/gmd-3-43-2010, 2010.

Emmons, L. K., Schwantes, R. H., Orlando, J. J., Tyndall, G., Kinnison, D., Lamarque, J. F., Marsh, D., Mills, M. J., Tilmes,
585   S., Bardeen, C., Buchholz, R. R., Conley, A., Gettelman, A., Garcia, R., Simpson, I., Blake, D. R., Meinardi, S., and Pétron, G.: The Chemistry Mechanism in the Community Earth System Model Version 2 (CESM2), Journal of Advances in Modeling Earth Systems, 12, 10.1029/2019ms001882, 2020.

Ervens, B.: Modeling the processing of aerosol and trace gases in clouds and fogs, Chem Rev, 115, 4157-4198, 10.1021/cr5005887, 2015.

590   Faloona, I.: Sulfur processing in the marine atmospheric boundary layer: A review and critical assessment of modeling uncertainties, Atmospheric Environment, 43, 2841-2854, 10.1016/j.atmosenv.2009.02.043, 2009.

Feng, L., Smith, S. J., Braun, C., Crippa, M., Gidden, M. J., Hoesly, R., Klimont, Z., van Marle, M., van den Berg, M., and van der Werf, G. R.: The generation of gridded emissions data for CMIP6, Geoscientific Model Development, 13, 461-482, 10.5194/gmd-13-461-2020, 2020.

Fenton, H. J. H.: LXXIII.—Oxidation of tartaric acid in presence of iron, Journal of the Chemical Society Transactions, 65, 899-910, 1894.

Flemming, J., Huijnen, V., Arteta, J., Bechtold, P., Beljaars, A., Blechschmidt, A. M., Diamantakis, M., Engelen, R. J., Gaudel, A., Inness, A., Jones, L., Josse, B., Katragkou, E., Marecal, V., Peuch, V. H., Richter, A., Schultz, M. G., Stein, O., and Tsikerdekis, A.: Tropospheric chemistry in the Integrated Forecasting System of ECMWF, Geoscientific Model Development, 8, 975-1003, 10.5194/gmd-8-975-2015, 2015.

Fritz, H., and Joseph, W.: The catalytic decomposition of hydrogen peroxide by iron salts, Proc. R. Soc. Lond. A147332–351, 10.1098/rspa.1934.0221, 1934.

Gankanda, A., Coddens, E. M., Zhang, Y., Cwiertny, D. M., and Grassian, V. H.: Sulfate formation catalyzed by coal fly ash, mineral dust and iron(iii) oxide: variable influence of temperature and light, Environ Sci Process Impacts, 18, 1484-1491, 10.1039/c6em00430j, 2016.

Geng, G., Xiao, Q., Zheng, Y., Tong, D., Zhang, Y., Zhang, X., Zhang, Q., He, K., and Liu, Y.: Impact of China's Air Pollution Prevention and Control Action Plan on $PM_{2.5}$ chemical composition over eastern China, Science China Earth Sciences, 62, 1872-1884, 10.1007/s11430-018-9353-x, 2019.

Georgiou, G. K., Christoudias, T., Proestos, Y., Kushta, J., Hadjinicolaou, P., and Lelieveld, J.: Air quality modelling in the summer over the eastern Mediterranean using WRF-Chem: chemistry and aerosol mechanism intercomparison, Atmospheric Chemistry and Physics, 18, 1555-1571, 10.5194/acp-18-1555-2018, 2018.

Gonzalez, D. H., Cala, C. K., Peng, Q., and Paulson, S. E.: HULIS Enhancement of Hydroxyl Radical Formation from Fe(II): Kinetics of Fulvic Acid-Fe(II) Complexes in the Presence of Lung Antioxidants, Environ Sci Technol, 51, 7676-7685, 10.1021/acs.est.7b01299, 2017.

Goto, D., Nakajima, T., Dai, T., Takemura, T., Kajino, M., Matsui, H., Takami, A., Hatakeyama, S., Sugimoto, N., Shimizu, A., and Ohara, T.: An evaluation of simulated particulate sulfate over East Asia through global model intercomparison, Journal of Geophysical Research: Atmospheres, 120, 6247-6270, 10.1002/2014jd021693, 2015.

Graedel, T. E., and Weschler, C. J.: Chemistry within Aqueous Atmospheric Aerosols and Raindrops, Rev Geophys, 19, 505-539, DOI 10.1029/RG019i004p00505, 1981.

Guo, H., Weber, R. J., and Nenes, A.: High levels of ammonia do not raise fine particle pH sufficiently to yield nitrogen oxide-dominated sulfate production, Sci Rep, 7, 12109, 10.1038/s41598-017-11704-0, 2017.

Guth, J., Josse, B., Marécal, V., Joly, M., and Hamer, P.: First implementation of secondary inorganic aerosols in the MOCAGE version R2.15.0 chemistry transport model, Geoscientific Model Development, 9, 137-160, 10.5194/gmd-9-137-2016, 2016.

Harris, E., Sinha, B., van Pinxteren, D., Tilgner, A., Fomba, K. W., Schneider, J., Roth, A., Gnauk, T., Fahlbusch, B., Mertes, S., Lee, T., Collett, J., Foley, S., Borrmann, S., Hoppe, P., and Herrmann, H.: Enhanced Role of Transition Metal Ion Catalysis During In-Cloud Oxidation of $SO_2$, Science, 340, 727-730, 10.1126/science.1230911, 2013.

He, G., Ma, J., and He, H.: Role of Carbonaceous Aerosols in Catalyzing Sulfate Formation, ACS Catalysis, 8, 3825-3832, 10.1021/acscatal.7b04195, 2018.

He, G., and He, H.: Water Promotes the Oxidation of $SO_2$ by $O_2$ over Carbonaceous Aerosols, Environ Sci Technol, 54, 7070-7077, 10.1021/acs.est.0c00021, 2020.

He, H., Wang, Y., Ma, Q., Ma, J., Chu, B., Ji, D., Tang, G., Liu, C., Zhang, H., and Hao, J.: Mineral dust and $NO_x$ promote the conversion of $SO_2$ to sulfate in heavy pollution days, Sci Rep, 4, 4172, 10.1038/srep04172, 2014.

He, J., Zhang, Y., Glotfelty, T., He, R., Bennartz, R., Rausch, J., and Sartelet, K.: Decadal simulation and comprehensive evaluation of CESM/CAM5.1 with advanced chemistry, aerosol microphysics, and aerosol-cloud interactions, Journal of Advances in Modeling Earth Systems, 7, 110-141, 10.1002/2014ms000360, 2015a.

He, J., Zhang, Y., Tilmes, S., Emmons, L., Lamarque, J. F., Glotfelty, T., Hodzic, A., and Vitt, F.: CESM/CAM5 improvement and application: comparison and evaluation of updated CB05_GE and MOZART-4 gas-phase mechanisms and associated impacts on global air quality and climate, Geoscientific Model Development, 8, 3999-4025, 10.5194/gmd-8-3999-2015, 2015b.

Heal, M. R., Hibbs, L. R., Agius, R. M., and Beverland, I. J.: Total and water-soluble trace metal content of urban background $PM_{10}$, $PM_{2.5}$ and black smoke in Edinburgh, UK, Atmospheric Environment, 39, 1417-1430, 10.1016/j.atmosenv.2004.11.026, 2005.

Hedegaard, G. B., Brandt, J., Christensen, J. H., Frohn, L. M., Geels, C., Hansen, K. M., and Stendel, M.: Impacts of climate change on air pollution levels in the Northern Hemisphere with special focus on Europe and the Arctic, Atmospheric Chemistry and Physics, 8, 3337-3367, DOI 10.5194/acp-8-3337-2008, 2008.

Herrmann, H., Ervens, B., Jacobi, H. W., Wolke, R., Nowacki, P., and Zellner, R.: CAPRAM2.3: A chemical aqueous phase radical mechanism for tropospheric chemistry, J Atmos Chem, 36, 231-284, Doi 10.1023/A:1006318622743, 2000.

Herrmann, H., Schaefer, T., Tilgner, A., Styler, S. A., Weller, C., Teich, M., and Otto, T.: Tropospheric aqueous-phase chemistry: kinetics, mechanisms, and its coupling to a changing gas phase, Chem Rev, 115, 4259-4334, 10.1021/cr500447k, 2015.

Hong, C., Zhang, Q., Zhang, Y., Tang, Y., Tong, D., and He, K.: Multi-year downscaling application of two-way coupled WRF v3.4 and CMAQ v5.0.2 over east Asia for regional climate and air quality modeling: model evaluation and aerosol direct effects, Geoscientific Model Development, 10, 2447-2470, 10.5194/gmd-10-2447-2017, 2017.

Hsu, S.-C., Liu, S. C., Arimoto, R., Shiah, F.-K., Gong, G.-C., Huang, Y.-T., Kao, S.-J., Chen, J.-P., Lin, F.-J., Lin, C.-Y., Huang, J.-C., Tsai, F., and Lung, S.-C. C.: Effects of acidic processing, transport history, and dust and sea salt loadings on the dissolution of iron from Asian dust, Journal of Geophysical Research, 115, 10.1029/2009jd013442, 2010.

655 Hsu, S.-C., Lin, F.-J., Liu, T.-H., Lin, S.-H., Kao, S.-J., Tseng, C.-M., and Huang, C.-H.: Short time dissolution kinetics of refractory elements Fe, Al, and Ti in Asian outflow-impacted marine aerosols and implications, Atmospheric Environment, 79, 93-100, 10.1016/j.atmosenv.2013.06.037, 2013.

Huang, L., An, J., Koo, B., Yarwood, G., Yan, R., Wang, Y., Huang, C., and Li, L.: Sulfate formation during heavy winter haze events and the potential contribution from heterogeneous $SO_2 + NO_2$ reactions in the Yangtze River Delta region, China,

660 Atmospheric Chemistry and Physics, 19, 14311-14328, 10.5194/acp-19-14311-2019, 2019.

Huang, L. B., Cochran, R. E., Coddens, E. M., and Grassian, V. H.: Formation of Organosulfur Compounds through Transition Metal Ion-Catalyzed Aqueous Phase Reactions, Environmental Science & Technology Letters, 5, 315-321, 10.1021/acs.estlett.8b00225, 2018.

Huang, X., Song, Y., Zhao, C., Li, M., Zhu, T., Zhang, Q., and Zhang, X.: Pathways of sulfate enhancement by natural and

665 anthropogenic mineral aerosols in China, Journal of Geophysical Research: Atmospheres, 119, 14,165-114,179, 10.1002/2014jd022301, 2014.

Hung, H. M., Hsu, M. N., and Hoffmann, M. R.: Quantification of $SO_2$ Oxidation on Interfacial Surfaces of Acidic Micro-Droplets: Implication for Ambient Sulfate Formation, Environ Sci Technol, 52, 9079-9086, 10.1021/acs.est.8b01391, 2018.

Im, U., Christensen, J. H., Geels, C., Hansen, K. M., Brandt, J., Solazzo, E., Alyuz, U., Balzarini, A., Baro, R., Bellasio, R.,

670 Bianconi, R., Bieser, J., Colette, A., Curci, G., Farrow, A., Flemming, J., Fraser, A., Jimenez-Guerrero, P., Kitwiroon, N., Liu, P., Nopmongcol, U., Palacios-Pena, L., Pirovano, G., Pozzoli, L., Prank, M., Rose, R., Sokhi, R., Tuccella, P., Unal, A., Vivanco, M. G., Yarwood, G., Hogrefe, C., and Galmarini, S.: Influence of anthropogenic emissions and boundary conditions on multi-model simulations of major air pollutants over Europe and North America in the framework of AQMEII3, Atmos Chem Phys, 18, 8929-8952, 10.5194/acp-18-8929-2018, 2018.

675 Ingall, E., Feng, Y., Longo, A., Lai, B., Shelley, R., Landing, W., Morton, P., Nenes, A., Mihalopoulos, N., Violaki, K., Gao, Y., Sahai, S., and Castorina, E.: Enhanced Iron Solubility at Low pH in Global Aerosols, Atmosphere, 9, 10.3390/atmos9050201, 2018.

Itahashi, S.: Toward Synchronous Evaluation of Source Apportionments for Atmospheric Concentration and Deposition of Sulfate Aerosol Over East Asia, Journal of Geophysical Research: Atmospheres, 123, 2927-2953, 10.1002/2017jd028110,

680 2018.

Itahashi, S., Yamaji, K., Chatani, S., and Hayami, H.: Refinement of Modeled Aqueous-Phase Sulfate Production via the Fe-and Mn-Catalyzed Oxidation Pathway, Atmosphere, 9, 10.3390/atmos9040132, 2018.

Jacob, D. J.: Chemistry of OH in Remote Clouds and Its Role in the Production of Formic-Acid and Peroxymonosulfate, J Geophys Res-Atmos, 91, 9807-9826, DOI 10.1029/JD091iD09p09807, 1986.

685 Jacob, D. J.: Heterogeneous chemistry and tropospheric ozone, Atmospheric Environment, 34, 2131-2159, Doi 10.1016/S1352-2310(99)00462-8, 2000.

Jo, Y.-J., Lee, H.-J., Jo, H.-Y., Woo, J.-H., Kim, Y., Lee, T., Heo, G., Park, S.-M., Jung, D., Park, J., and Kim, C.-H.: Changes in inorganic aerosol compositions over the Yellow Sea area from impact of Chinese emissions mitigation, Atmospheric Research, 240, 10.1016/j.atmosres.2020.104948, 2020.

690 Kajino, M., Deushi, M., Maki, T., Oshima, N., Inomata, Y., Sato, K., Ohizumi, T., and Ueda, H.: Modeling wet deposition and concentration of inorganics over Northeast Asia with MRI-PM/c, Geoscientific Model Development, 5, 1363-1375, 10.5194/gmd-5-1363-2012, 2012.

Kan, H., Chen, R., and Tong, S.: Ambient air pollution, climate change, and population health in China, Environ Int, 42, 10-19, 10.1016/j.envint.2011.03.003, 2012.

695 Lakey, P. S., George, I. J., Baeza-Romero, M. T., Whalley, L. K., and Heard, D. E.: Organics Substantially Reduce $HO_2$ Uptake onto Aerosols Containing Transition Metal ions, J Phys Chem A, 120, 1421-1430, 10.1021/acs.jpca.5b06316, 2016.

Lamarque, J. F., Emmons, L. K., Hess, P. G., Kinnison, D. E., Tilmes, S., Vitt, F., Heald, C. L., Holland, E. A., Lauritzen, P. H., Neu, J., Orlando, J. J., Rasch, P. J., and Tyndall, G. K.: CAM-chem: description and evaluation of interactive atmospheric chemistry in the Community Earth System Model, Geoscientific Model Development, 5, 369-411, 10.5194/gmd-5-369-2012,

700 2012.

Lee, Y. N., and Schwartz, S. E.: Kinetics of oxidation of aqueous sulfur(IV) by nitrogen dioxide, 1982.

Li, G., Bei, N., Cao, J., Huang, R., Wu, J., Feng, T., Wang, Y., Liu, S., Zhang, Q., Tie, X., and Molina, L. T.: A possible pathway for rapid growth of sulfate during haze days in China, Atmospheric Chemistry and Physics, 17, 3301-3316, 10.5194/acp-17-3301-2017, 2017.

705 Li, J., Chen, X., Wang, Z., Du, H., Yang, W., Sun, Y., Hu, B., Li, J., Wang, W., Wang, T., Fu, P., and Huang, H.: Radiative and heterogeneous chemical effects of aerosols on ozone and inorganic aerosols over East Asia, Sci Total Environ, 622-623, 1327-1342, 10.1016/j.scitotenv.2017.12.041, 2018a.

Li, J., Zhang, Y. L., Cao, F., Zhang, W., Fan, M., Lee, X., and Michalski, G.: Stable Sulfur Isotopes Revealed a Major Role of Transition-Metal Ion-Catalyzed $SO_2$ Oxidation in Haze Episodes, Environ Sci Technol, 54, 2626-2634,

710 10.1021/acs.est.9b07150, 2020.

Li, L., Hoffmann, M. R., and Colussi, A. J.: Role of Nitrogen Dioxide in the Production of Sulfate during Chinese Haze-Aerosol Episodes, Environ Sci Technol, 52, 2686-2693, 10.1021/acs.est.7b05222, 2018b.

Liang, J. Y., and Jacobson, M. Z.: A study of sulfur dioxide oxidation pathways over a range of liquid water contents, pH values, and temperatures, J Geophys Res-Atmos, 104, 13749-13769, Doi 10.1029/1999jd900097, 1999.

715 Liu, F., Choi, S., Li, C., Fioletov, V. E., McLinden, C. A., Joiner, J., Krotkov, N. A., Bian, H., Janssens-Maenhout, G., Darmenov, A. S., and da Silva, A. M.: A new global anthropogenic $SO_2$ emission inventory for the last decade: a mosaic of satellite-derived and bottom-up emissions, Atmospheric Chemistry and Physics, 18, 16571-16586, 10.5194/acp-18-16571-2018, 2018.

Liu, J., Horowitz, L. W., Fan, S., Carlton, A. G., and Levy, H.: Global in-cloud production of secondary organic aerosols: Implementation of a detailed chemical mechanism in the GFDL atmospheric model AM3, Journal of Geophysical Research: Atmospheres, 117, 10.1029/2012jd017838, 2012a.

Liu, X., Penner, J. E., Das, B., Bergmann, D., Rodriguez, J. M., Strahan, S., Wang, M., and Feng, Y.: Uncertainties in global aerosol simulations: Assessment using three meteorological data sets, Journal of Geophysical Research, 112, 10.1029/2006jd008216, 2007.

Liu, X., Easter, R. C., Ghan, S. J., Zaveri, R., Rasch, P., Shi, X., Lamarque, J. F., Gettelman, A., Morrison, H., Vitt, F., Conley, A., Park, S., Neale, R., Hannay, C., Ekman, A. M. L., Hess, P., Mahowald, N., Collins, W., Iacono, M. J., Bretherton, C. S., Flanner, M. G., and Mitchell, D.: Toward a minimal representation of aerosols in climate models: description and evaluation in the Community Atmosphere Model CAM5, Geoscientific Model Development, 5, 709-739, 10.5194/gmd-5-709-2012, 2012b.

Ma, J., Chu, B., Liu, J., Liu, Y., Zhang, H., and He, H.: $NO_x$ promotion of $SO_2$ conversion to sulfate: An important mechanism for the occurrence of heavy haze during winter in Beijing, Environ Pollut, 233, 662-669, 10.1016/j.envpol.2017.10.103, 2018.

Mao, J., Fan, S., Jacob, D. J., and Travis, K. R.: Radical loss in the atmosphere from Cu-Fe redox coupling in aerosols, Atmospheric Chemistry and Physics, 13, 509-519, 10.5194/acp-13-509-2013, 2013.

Mao, J., Fan, S., and Horowitz, L. W.: Soluble Fe in Aerosols Sustained by Gaseous $HO_2$ Uptake, Environmental Science & Technology Letters, 4, 98-104, 10.1021/acs.estlett.7b00017, 2017.

Mathur, R.: Multiscale Air Quality Simulation Platform (MAQSIP): Initial applications and performance for tropospheric ozone and particulate matter, Journal of Geophysical Research, 110, 10.1029/2004jd004918, 2005.

Matthijsen, J., Builtjes, P. J. H., and Sedlak, D. L.: Cloud Model Experiments of the Effect of Iron and Copper on Tropospheric Ozone under Marine and Continental Conditions, Meteorol Atmos Phys, 57, 43-60, Doi 10.1007/Bf01044153, 1995.

McDaniel, M. F. M., Ingall, E. D., Morton, P. L., Castorina, E., Weber, R. J., Shelley, R. U., Landing, W. M., Longo, A. F., Feng, Y., and Lai, B.: Relationship between Atmospheric Aerosol Mineral Surface Area and Iron Solubility, ACS Earth and Space Chemistry, 3, 2443-2451, 10.1021/acsearthspacechem.9b00152, 2019.

Myriokefalitakis, S., Ito, A., Kanakidou, M., Nenes, A., Krol, M. C., Mahowald, N. M., Scanza, R. A., Hamilton, D. S., Johnson, M. S., Meskhidze, N., Kok, J. F., Guieu, C., Baker, A. R., Jickells, T. D., Sarin, M. M., Bikkina, S., Shelley, R., Bowie, A., Perron, M. M. G., and Duce, R. A.: Reviews and syntheses: the GESAMP atmospheric iron deposition model intercomparison study, Biogeosciences, 15, 6659-6684, 10.5194/bg-15-6659-2018, 2018.

Pang, S. Y., Jiang, J., and Ma, J.: Oxidation of Sulfoxides and Arsenic(III) in Corrosion of Nanoscale Zero Valent Iron by Oxygen: Evidence against Ferryl Ions (Fe(IV)) as Active Intermediates in Fenton Reaction, Environmental Science & Technology, 45, 307-312, 10.1021/es102401d, 2011.

Ponche, J. L., George, C., and Mirabel, P.: Mass-Transfer at the Air-Water-Interface - Mass Accommodation Coefficients of

750    $SO_2$, $HNO_3$, $NO_2$ and $NH_3$, J Atmos Chem, 16, 1-21, Doi 10.1007/Bf00696620, 1993.

Poschl, U., and Shiraiwa, M.: Multiphase chemistry at the atmosphere-biosphere interface influencing climate and public

health in the anthropocene, Chem Rev, 115, 4440-4475, 10.1021/cr500487s, 2015.

Pozzer, A., de Meij, A., Pringle, K. J., Tost, H., Doering, U. M., van Aardenne, J., and Lelieveld, J.: Distributions and regional

budgets of aerosols and their precursors simulated with the EMAC chemistry-climate model, Atmospheric Chemistry and

755    Physics, 12, 961-987, 10.5194/acp-12-961-2012, 2012.

Quan, J., Liu, Q., Li, X., Gao, Y., Jia, X., Sheng, J., and Liu, Y.: Effect of heterogeneous aqueous reactions on the secondary

formation of inorganic aerosols during haze events, Atmospheric Environment, 122, 306-312, 10.1016/j.atmosenv.2015.09.068,

2015.

Rudich, Y., Talukdar, R. K., Ravishankara, A. R., and Fox, R. W.: Reactive uptake of $NO_3$ on pure water and ionic solutions,

760    Journal of Geophysical Research: Atmospheres, 101, 21023-21031, 10.1029/96jd01844, 1996.

Sedwick, P. N., Sholkovitz, E. R., and Church, T. M.: Impact of anthropogenic combustion emissions on the fractional

solubility of aerosol iron: Evidence from the Sargasso Sea, Geochemistry, Geophysics, Geosystems, 8, 10.1029/2007gc001586,

2007.

Seinfeld, J. H., and Pandis, S. N.: Atmospheric Chemistry and Physics: From Air Pollution to Climate Change. 2nd edition,

765    2006.

Sha, T., Ma, X., Jia, H., Tian, R., Chang, Y., Cao, F., and Zhang, Y.: Aerosol chemical component: Simulations with WRF-

Chem and comparison with observations in Nanjing, Atmospheric Environment, 218, 10.1016/j.atmosenv.2019.116982, 2019.

Shao, J., Chen, Q., Wang, Y., Lu, X., He, P., Sun, Y., Shah, V., Martin, R. V., Philip, S., Song, S., Zhao, Y., Xie, Z., Zhang, L.,

and Alexander, B.: Heterogeneous sulfate aerosol formation mechanisms during wintertime Chinese haze events: air quality

770    model assessment using observations of sulfate oxygen isotopes in Beijing, Atmospheric Chemistry and Physics, 19, 6107-

6123, 10.5194/acp-19-6107-2019, 2019.

Shelley, R. U., Landing, W. M., Ussher, S. J., Planquette, H., and Sarthou, G.: Regional trends in the fractional solubility of Fe

and other metals from North Atlantic aerosols (GEOTRACES cruises GA01 and GA03) following a two-stage leach,

Biogeosciences, 15, 2271-2288, 10.5194/bg-15-2271-2018, 2018.

775    Shi, G., Xu, J., Shi, X., Liu, B., Bi, X., Xiao, Z., Chen, K., Wen, J., Dong, S., Tian, Y., Feng, Y., Yu, H., Song, S., Zhao, Q.,

Gao, J., and Russell, A. G.: Aerosol pH Dynamics During Haze Periods in an Urban Environment in China: Use of Detailed,

Hourly, Speciated Observations to Study the Role of Ammonia Availability and Secondary Aerosol Formation and Urban

Environment, Journal of Geophysical Research: Atmospheres, 124, 9730-9742, 10.1029/2018jd029976, 2019.

Shi, J., Guan, Y., Ito, A., Gao, H., Yao, X., Baker, A. R., and Zhang, D.: High Production of Soluble Iron Promoted by Aerosol

780    Acidification in Fog, Geophysical Research Letters, 47, 10.1029/2019gl086124, 2020.

Sholkovitz, E. R., Sedwick, P. N., and Church, T. M.: Influence of anthropogenic combustion emissions on the deposition of soluble aerosol iron to the ocean: Empirical estimates for island sites in the North Atlantic, Geochimica et Cosmochimica Acta, 73, 3981-4003, 10.1016/j.gca.2009.04.029, 2009.

785 Tan, J., Duan, J., Zhen, N., He, K., and Hao, J.: Chemical characteristics and source of size-fractionated atmospheric particle in haze episode in Beijing, Atmospheric Research, 167, 24-33, 10.1016/j.atmosres.2015.06.015, 2016.

Tang, M., Cziczo, D. J., and Grassian, V. H.: Interactions of Water with Mineral Dust Aerosol: Water Adsorption, Hygroscopicity, Cloud Condensation, and Ice Nucleation, Chem Rev, 116, 4205-4259, 10.1021/acs.chemrev.5b00529, 2016.

Tao, J., Zhang, L., Cao, J., and Zhang, R.: A review of current knowledge concerning $PM_{2.5}$ chemical composition, aerosol optical properties and their relationships across China, Atmospheric Chemistry and Physics, 17, 9485-9518, 10.5194/acp-17-
790 9485-2017, 2017.

Tilgner, A., Bräuer, P., Wolke, R., and Herrmann, H.: Modelling multiphase chemistry in deliquescent aerosols and clouds using CAPRAM3.0i, J Atmos Chem, 70, 221-256, 10.1007/s10874-013-9267-4, 2013.

Tong, H., Lakey, P. S. J., Arangio, A. M., Socorro, J., Kampf, C. J., Berkemeier, T., Brune, W. H., Poschl, U., and Shiraiwa, M.: Reactive oxygen species formed in aqueous mixtures of secondary organic aerosols and mineral dust influencing cloud
795 chemistry and public health in the Anthropocene, Faraday Discuss, 200, 251-270, 10.1039/c7fd00023e, 2017.

Wang, J., Li, J., Ye, J., Zhao, J., Wu, Y., Hu, J., Liu, D., Nie, D., Shen, F., Huang, X., Huang, D. D., Ji, D., Sun, X., Xu, W., Guo, J., Song, S., Qin, Y., Liu, P., Turner, J. R., Lee, H. C., Hwang, S., Liao, H., Martin, S. T., Zhang, Q., Chen, M., Sun, Y., Ge, X., and Jacob, D. J.: Fast sulfate formation from oxidation of $SO_2$ by $NO_2$ and HONO observed in Beijing haze, Nat Commun, 11, 2844, 10.1038/s41467-020-16683-x, 2020.

800 Wang, R., Balkanski, Y., Boucher, O., Bopp, L., Chappell, A., Ciais, P., Hauglustaine, D., Peñuelas, J., and Tao, S.: Sources, transport and deposition of iron in the global atmosphere, Atmospheric Chemistry and Physics, 15, 6247-6270, 10.5194/acp-15-6247-2015, 2015.

Warneck, P.: The oxidation of sulfur(iv) by reaction with iron(iii): a critical review and data analysis, Phys Chem Chem Phys, 20, 4020-4037, 10.1039/c7cp07584g, 2018.

805 Wei, Y., Chen, X., Chen, H., Li, J., Wang, Z., Yang, W., Ge, B., Du, H., Hao, J., Wang, W., Li, J., Sun, Y., and Huang, H.: IAP-AACM v1.0: a global to regional evaluation of the atmospheric chemistry model in CAS-ESM, Atmospheric Chemistry and Physics, 19, 8269-8296, 10.5194/acp-19-8269-2019, 2019.

Wiegand, H. L., Orths, C. T., Kerpen, K., Lutze, H. V., and Schmidt, T. C.: Investigation of the Iron-Peroxo Complex in the Fenton Reaction: Kinetic Indication, Decay Kinetics, and Hydroxyl Radical Yields, Environ Sci Technol, 51, 14321-14329,
810 10.1021/acs.est.7b03706, 2017.

Xie, X., Liu, X., Wang, H., and Wang, Z.: Effects of Aerosols on Radiative Forcing and Climate Over East Asia With Different $SO_2$ Emissions, Atmosphere, 7, 10.3390/atmos7080099, 2016.